Title

Emergent feedforward and isohydric responses to soil and atmospheric aridity: Insights from a time-dependent hydraulic model.

Author list

Fulton E. Rockwell

Affiliations

Corresponding author and email

Fulton E. Rockwell, fulton.rockwell@gmail.com

Orcids: 0000-0002-2527-6033

Summary

Drought and heat waves have synergistic effects on mortality as plants experience both supply and demand-side water stress. Which of these stresses ultimately controls stomatal conductance (g_s) and whether patterns of regulation represent biological strategies or are imposed on the plant are addressed by way of a mechanistic hydraulic 'null' model.

- Dynamic losses of soil hydraulic conductivity are modeled in a soil domain fed by a maximum water flux from a deep-water source. A root-uptake plane extracts water from the soil in a two-node (root and leaf) plant model, with g_s a function of leaf water potential.

- Multi-day simulations reproduce previously published experimental observations of anisohydric to isohydric transitions, driven by the balance of soil supply and atmospheric demand. Feedforward control of transpiration E emerges from steep declines in soil hydraulic diffusivity that confine diurnal variation in moisture gradients and water discharge/recharge cycles to a shallow region at the root plane that thins with increased demand.

- Empirical models of VPD sensitivity are compared to the full model to provide mechanistic insight into empirical parameters. Apparent responses of g_s to VPD are shown to emerge from plant, soil and atmospheric feedbacks that are both time and scale dependent.

Keywords [drought, vapor pressure deficit, soil hydraulics, stomatal conductance, feedforward stomatal control, stomatal response to vpd]

Table of word counts each section (I, MD, R, D). Num figs. Num Tables, num SI.

Total word count	7495	No. of Figures	8
Introduction	1635	No. of Tables	0
Model Description	1570	No. of Supporting Information files	3
Results	2585		
Discussion	1705		

Introduction

The dual role of stomata in admitting an inward flux of CO_2 while preventing the desiccation of plant tissues has been recognized at least since Van Den Honert (1948), who proposed that stomata serve as the dominant resistance to water transport in the soil-plant-atmosphere continuum (‘SPAC’; Philip, 1966). While guard cells, as hydraulicly actuated valves, respond ‘passively’ to local water status, pore aperture is also decoupled from the local water potential of the epidermis by ‘active’ biochemistry (e.g., light activated ion pumping, ABA induced closure; McAdam & Brodribb, 2016; Jezek & Blatt, 2017), with the resulting complexity of regulation obscuring the control points that sense water status and govern stomatal behavior (Tardieu & Simonneau, 1998; Buckley, 2005; McAdam & Brodribb, 2016; Novick *et al.*, 2019; Jezek *et al.*, 2019; Grossiord *et al.*, 2020; Wankmüller & Carminati, 2022). While the twin stressors of heat and drought are known to have synergistic mortality effects (Mitchell *et al*., 2014; Matusick *et al*., 2018), the lack of a clear understanding of how stomata integrate supply and demand stresses has led to controversy regarding plant responses to future climates, a debate focused on whether stomatal conductance is more limited by available soil water or atmospheric aridity (Roderick *et al.*, 2015; Novick *et al.*, 2016a, 2024; Berg & Sheffield, 2018; Grossiord *et al.*, 2020; Liu *et al.*, 2020a; McColl & Tang, 2024).

The biologically ‘active’ nature of stomatal regulation suggests that the 60% of global terrestrial evapotranspiration mediated by plant canopies is subject to a diversity of stomatal control strategies varying across species, functional groups and biomes (Tardieu & Simonneau, 1998;

Oren *et al.*, 1999; Martinez-Vilalta & Garcia-Forner, 2017; Novick *et al*., 2019; Wu *et al*., 2021). Yet, caught between Equivalent Water Thicknesses (EWT) for both the unsaturated soil zone and atmosphere on the order of centimeters, the plant canopy with an EWT on the order of millimeters may have little scope to express independent control of its water status at equilibrium (Shiklomanov, 1993; Hunt, Jr. *et al.*, 2009). The behavior of the plant canopy may then follow that of any 'passive' material that loses conductivity as it dries (Hochberg *et al*., 2018; Feng *et al*., 2019; Vargas Zeppetello *et al*., 2023). With respect to the global water cycle, the plant canopy may approximate ‘green dirt.’

Physiologically, interest in vapor pressure deficit (*VPD*) responses as distinct from source water limitations accelerated with evidence of ‘feed-forward’ stomatal behavior: stomatal closure that does not merely reduce increases in transpiration *E* with increases in atmospheric demand, but results in *lower E* (Cowan & Troughton, 1971). Such behavior cannot be explained by local hydraulic resistances that create steady-state feed-backs of *E* on guard cell water potential and stomatal apertures. Local feed-backs describe an incremental draw-down in water potential resulting from an incremental *increase* in *E*, thereby reducing the realized increase in *E* but not *E* itself (Cowan & Troughton, 1971; Franks *et al.*, 1997,1999; Buckley, 2005). The inadequacy of local hydraulic feedbacks, together with demonstrations that leaf water potential and stomatal conductance do not follow a one-to-one relationship, has turned attention toward metabolic and chemical controls on stomatal responses to water stress (Turner *et al.*, 1984, 1985; Gollan *et al.*, 1985; Simonneau & Tardieu, 1998; McAdam & Brodribb, 2016).

This change of research focus makes sense: the principal activity of guard cell physiology is to break any one-to-one relationship of stomatal pore aperture to water potential by manipulating ion concentrations in response to an array of signals and forcings, including ABA, photon flux density, light quality, substrate availability, enzyme activation, CO_2 concentrations and temperature (Schroeder *et al.*, 2001; Messinger *et al.*, 2006; Brodribb & McAdam, 2011; Buckley, 2019; Jezek *et al.*, 2019). Despite, or perhaps because of the richness of physiological detail that has been described at the guard cell level, efforts to predict whole plant responses to environmental forcing at scale have adopted empirical approaches that produce behavior consistent with physiological response patterns but do not require mechanistic closure (Anderegg

et al., 2017; Mrad *et al.*, 2019; Grossiord *et al.*, 2020; Wang *et al.*, 2020; Mencuccini *et al.*, 2024).

The most widely adopted empirical approach to partitioning changes in stomatal aperture between supply and demand limitation has been to model maximum stomatal conductance ($g_{s,\mathrm{ref}}$) as a function of soil moisture, and fit a slope parameter (m) that describes the erosion of conductance with increasing vapor pressure deficit (*VPD*) (Oren *et al.*, 1999; Novick *et al.*, 2016a, 2019; Grossiord *et al.*, 2020). This approach has attracted the criticism that soil moisture and *VPD* are not independent at the spatial and temporal scales relevant to climate (Roderick *et al.*, 2015; Novick *et al.*, 2016a; Berg & Sheffield, 2018; Liu *et al.*, 2020a). Even at the sub-daily physiological scale of flux tower data over which bulk soil moisture and *VPD* are more weakly correlated (Novick *et al.*, 2024) it is unclear to what extent apparent stomatal responses to *VPD* are truly independent of soil moisture stress (Novick *et al.*, 2019; Koehler *et al.*, 2024), and so whether parameterizing independent soil and *VPD* responses amounts to double counting (Liu *et al.*, 2020b).

At daily time scales, an empirical approach has been developed that predicts E and surface conductance solely from weather data. The ETRHEQ hypothesis (EvapoTranspiration from Relative Humidity at Equilibrium) minimizes the vertical variance of RH through the Atmospheric Boundary Layer (ABL) to find the surface conductance (interpreted as g_s; Grossiord *et al.*, 2020). ETRHEQ can then be used to construct a response of g_s to *VPD* (Salvucci & Gentine, 2013; Rigden & Salvucci, 2015). As an empirical steady-state theory, ETRHEQ does not specify the mechanisms driving the relationships it describes. To address this gap, McColl *et al*. (2019) and McColl & Rigden (2020) provided a simple theory of Surface Flux Equilibrium (SFE) that relates the RH of the ABL to the balance of latent and sensible heat at the surface. As the system evolves toward an ‘equilibrium’ steady-state at which inputs from the surface match the fluxes out of the top of the ABL, the state of the land surface becomes fully reflected in the state of the atmosphere over time scales ranging from daily for ‘wet’ surfaces, to somewhat longer for ‘dry’ surfaces (McColl & Rigden, 2020).

SFE does not necessarily offer a unique explanation for ETRHEQ, nor can it establish the direction of causality between RH and g_s based on their internal relationship in the stationary-state. What SFE does do is capture the ETRHEQ hypothesis in a model that includes feedbacks

on E due to humidification and heating of the atmosphere by the surface heat and moisture fluxes, without imposing a prescribed biological response of g_s to *VPD*. The success of SFE/ETRHEQ begs the question of whether surface conductance is determined by active biological optimization and adaptive strategies for stress avoidance, or is primarily physically constrained (Konings & Gentine, 2017; Wu *et al.*, 2021; Vargas Zeppetello *et al.*, 2023; Mencuccini *et al.*, 2024), a gap in understanding that has led to calls for further work on the problem (Novick et al., 2019; Grossiord et al., 2020). There is also continued related uncertainty as to whether the isohydric-anisohydric spectrum of behavior describes biological adaptation, or reflects physical limits imposed on the plant by soil and atmospheric aridity (Konings & Gentine, 2017; Martínez-Vilalta & Garcia-Forner, 2017; Hochberg *et al.*, 2018; Feng *et al.*, 2019; Novick *et al.*, 2019; Wu *et al.*, 2021; Mencuccini *et al.*, 2024).

One element often missing from these debates is an appropriate 'null model' for environmental control of stomatal conductance that might be employed to separate biological versus purely physical regulation of E (Hochberg *et al.*, 2018; Carminati & Javaux, 2020; Rodriguez-Dominguez & Brodribb, 2020; Vargas Zeppetello *et al.*, 2023; Manandhar *et al.*, 2024; Mencuccini *et al.*, 2024). Toward this end, this study develops a time-dependent SPAC model from a continuum approach to soil water transport coupled to an ohmic (discrete) plant with stomatal conductance responding solely to leaf water potential. The goal is not to build an exhaustive mechanistic model of water and CO_2 fluxes in the SPAC (Tuzet *et al.*, 2003), nor to provide a sub-model appropriate for incorporation into large-scale land surface and atmosphere models (Sloan *et al.*, 2021). Rather the aim is to construct a minimal hydraulic representation of the SPAC for understanding environmental contributions to experimentally observed patterns of transpiration. Such a model may help resolve the physical factors contributing to the fitted parameters in scalable empirical models of stomatal responses to *VPD* and soil drought (Attia *et al.*, 2015; Konings & Gentine, 2017; Novick *et al.*, 2019; Mrad *et al.*, 2019; Grossiord *et al.*, 2020; Mencuccini *et al.*, 2024).

The null model developed here is first employed to test whether a minimal hydraulic time-dependent approach can successfully recover observations of 1) intra-day feed-forward stomatal behavior in response to diurnally varying *VPD*, 2) conservation of total daily transpiration across days and *VPD* levels, and 3) isohydric midday leaf water potentials in response to a

doubling of *VPD*, as previously observed in a whole-tree chamber experiment (Drake *et al.*, 2018). As in leaf-level studies of VPD responses using gas exchange cuvettes that minimize boundary layer effects (Franks *et al.*, 1997; Mott & Parkhurst, 1991), whole tree chambers allow the isolation of stomatal responses to stress *in situ* and at the whole plant level. The model is then employed to explore the effectiveness of a hypothetical osmotic adjustment to maintain carbon gain, and a sensitivity analysis is undertaken to understand the basis for the emergence of feed-forward and aniso/isohydric behavior from soil water dynamics. Finally, two empirical steady-state models are compared for their ability to capture the patterns of stomatal sensitivity to *VPD* that emerge over physiological (hourly) versus diel (daily) time scales, and these are then compared to the patterns expected under SFE over multiday time scales.

Model Description

Model structure and analysis of basic behavior

In SPAC models the three-dimensional transfer of water from soil to roots and from leaves to the atmosphere is collapsed into a single dimension. Here, time-dependent flow in the soil is modeled in cartesian rather than cylindrical coordinates (See Supplemental Information Notes **S1** for a full discussion and derivation). The extra 'resistance' created by the concentration of the flux as it approaches the root surface is neglected, which for the purposes of demonstrating soil constraints on transpiration is a conservative choice. The dynamics of infiltration by rainfall into the soil domain are not modeled; in principle meteoric inputs re-set the initial condition for soil moisture with which the model is run. As in general the soil is wetter below the root zone as plants extract water during meteoric drought (Miguez-Macho & Fan, 2021), the model domain is fed at the lower boundary by an asymptotic (maximum) soil flux determined by soil properties and the effective depth L (m) to a deep source of soil moisture (Gardner, 1958; Gardner & Fireman, 1958; Jury *et al*., 1991). A rooting surface located at a characteristic depth bounds the top of the model domain (Supplemental Information Notes S1; Binks *et al*., 2022), serving as a sink driven by transpiration through a discrete plant composed of two nodes (root and leaf water potential) separated by a whole plant conductance (Fig. **1a**). The neglect of plant capacitance follows Cowan's (1965) arguments that soil capacitance is expected to dominate the time scale of storage effects. Plant hydraulic conductance K_{plant} is held constant based on the hypothesis that

stomatal closure precedes cavitation (Hochberg *et al.*, 2017), while varying tissue hydraulic conductivity lies outside the scope of a minimal physical model.

Transpiration is represented as the product of a peak transpiration rate (E_p) that carries the units of cm day^{-1} with three dimensionless factors that introduce variations into E. The first is a diurnal demand function $f(t)$ (Fig. **1b**) that produces a sinusoidal range from 0 to 1, representing the effects of diurnal variations in air temperature on *VPD* in the well mixed air above the canopy as well as variations in stomatal aperture as light levels change over the day. The second is a non-dimensional nominal *VPD* level (*nVPD*) that represents daily peak atmospheric sink strength, and the third is a non-dimensional total conductance (stomatal plus boundary layer, scaled 0 to 1) that depends on leaf water potential and captures the effect of water stress on the realized evaporation rate (Fig. **1c**). In this framework, it is useful to distinguish between 'Potential transpiration' *PE*, which represents the transpiration rate that would be realized at maximum total conductance, and the actual transpiration E inclusive of stomatal water limitation effects,

$$PE = E_p\, nVPD\, (1 - \cos 2\pi t/\tau_d), \qquad eq.1$$

$$E = E_p\, nVPD\, g_{tot}(\Psi)\, (1 - \cos 2\pi t/\tau_d), \quad g_{tot} = \left[\frac{1}{g_s(\Psi)} + \frac{1}{g_{bl}}\right]^{-1} \qquad eq.2$$

where τ_d is the period of diel oscillation of one day.

In the soil domain changes in water content are related to changes in hydraulic conductivity and flux by Richard's equation (Fig. **1d**), neglecting gravitational effects over the centimeter scale (Cowan, 1965). The governing equation, boundary conditions, and initial conditions are then linearized using the Kirchhoff transform, leading to the expression of soil water content θ, soil matric potential h, and leaf water potential Ψ in terms of a single variable φ, a potential flux with diffusive units of cm^2 day^{-1}. To organize all the parameters in the model into dimensionless groups that describe the behavior of the solution, φ, time t and length z, are re-scaled to express the governing equations and boundary conditions as functions of the non-dimensional potential flux $\Phi = \varphi/(H\, J_m)$, time $T = t/\tau_d$, and length $Z = z/H$, where H is the height of the model domain:

$$\frac{\partial \Phi}{\partial T} = \frac{\tau_d}{\tau_s}\Phi\frac{\partial^2 \Phi}{\partial Z^2}, \quad \tau_d = 1, \quad \tau_s = \frac{H}{J_m D_o}. \qquad eq.3$$

$$-\frac{\partial \Phi}{\partial Z}|_{Z=0} = 1. \qquad eq.4$$

$$-\frac{\partial \Phi}{\partial Z}|_{Z=1} = \beta\, g_s(\Phi)\,(1-\cos 2\pi T), \quad \beta = \frac{E_p\, nVPD}{2\, J_m}. \qquad eq.5$$

$$\Phi(0,Z) = \frac{1}{H\, J_m}. \qquad eq.6$$

The model takes the form of a non-linear diffusion equation, where the soil diffusivity, $D(\Phi)=D_o\Phi$, introduces non-linearity through its dependence on the potential flux itself (note that D_o is a pure number that sets the initial magnitude of the soil diffusivity). Conceptually, soil diffusivity represents a ratio of hydraulic conductivity to hydraulic capacity (water storage).

There are two timescales in the problem (eq. 3). The first is the period of oscillations in potential transpiration of one day, τ_d (eq. 2). The second is the diffusive timescale τ_s, the characteristic time for the soil domain to attain a new steady state after a perturbation at the boundary, which is larger (slower) for larger domain sizes (H) and lower fluxes from the water source J_m. Larger values of D_o mean that conductance dominates soil capacitance contributing to faster response times (damping is low), while smaller values mean soil capacitance dominates conductance, slowing response times (damping is high). These two timescales appear as a ratio, meaning their relative values determine the time-dependent behavior of the model. However, this behavior is not entirely predictable as $D_o\Phi$ varies with time and position in the soil domain, with important consequences.

The remaining parameter driving model behavior is β (eq. 5). β represents the balance of potential evaporation *PE* to a steady asymptotic flux into the soil domain. As the value of the time-varying term in eq. 5 integrated over a single day is 1, a β of 1 means that the *total daily* flux from the source (eq. 4, always equal to 1) balances *total daily PE*, allowing normalized stomatal conductance to remain near its maximum value of 1. Yet, even under this daily balance of supply and demand peak potential transpiration rate exceeds the steady flux into the soil domain by a factor of 2. Such excess demand can be met by the discharge of soil water as φ falls in the domain, and stomatal closure need not occur over the course of the day. If the inward flux from the source is sufficient to re-charge the soil domain overnight, a cycle of daily peak *E* exceeding the inward flux without stomatal limitation can continue. For β >1, stomatal regulation

will at some point be triggered according to the scale of the imbalance and the ratio of timescales. But there is nothing in the model that forces a balance of inputs and outputs at the daily scale. It is helpful to keep in mind that the *instantaneous* balance of supply and demand seen by the plant is the sum of a steady inward soil flux that originates outside the domain and a transient capacitive or storage flux that originates within the domain. This combined flux can become asymptotic at the root plane at an emergent maximum *larger* than the maximum steady inward flux at the lower domain boundary that is represented in β. Note that β is numerically equivalent to *nVPD.*

Parameterization for the Drake experiment

In the Drake *et al.* (2018) experiment, individual eucalyptus trees (~ 6 m tall) were enclosed in 9 m tall temperature and humidity-controlled gas exchange chambers (CO_2, H_2O). The experiment subjected pre-droughted trees to a 'Heat Wave' treatment, combining air temperature (daily peak 43-44°C) and *VPD* stress (daily peak 5-6 kPa), versus a 'Control' subject to typical conditions (daily peaks of 28-29 ^{o}C, 2-2.5 kPa). Irrigation was withheld, making ground water the only possible source recharging the soil domain. As the trees were enclosed in well-stirred air, total canopy conductance was close to stomatal conductance and leaf temperature close to air temperature (*e.g.*, Fig. 4 in Drake *et al.*, 2018), such that atmospheric humidity was 'imposed' at the leaf surface (Jarvis & McNaughton, 1986). The potential transpiration rate E_p was set to 0.3 cm day^{-1} to match the intraday peak of 2 mmol m^{-2} s^{-1} seen in the controls (Drake *et al.*, 2018; Fig. 2c). Peak *VPD* for the controls (~ 3 kPa) was set as the reference value for normalizing *VPD*. The maximum flux from the water table J_m was set to half of E_p, 0.15 cm day^{-1} in accord with the definition of β=1 at *nVPD*=1 (eq. 5). Stomatal conductance is given by a sigmoidal function of leaf water potential (Anderegg *et al*., 2017; Franks & Farquhar, 2007; Levin *et al*., 2019). The shape parameter *b* (MPa) and water potential for 50% stomatal closure ($g_s\Psi_{50}$) were fit together with total plant hydraulic conductance (K_{plant}; cm day^{-1} MPa^{-1}) to reproduce the midday water potentials reported in Drake *et al.*, (2018). Stomatal conductance transforms to Φ (and $g_s\Psi_{50}$ to $g_s\Phi_{50}$) as,

$$g_s(\Phi) = \left(1 + exp\left[\left(\frac{-430.11\,\rho g}{HJ_m g_s \Phi_{50}} - \left(\frac{-430.11\,\rho g}{HJ_m \Phi|_{Z=1}} + \frac{J_m \partial\Phi/\partial Z\big|_{Z=1}}{K_{plant}}\right)\right)\Big/ b\right]\right)^{-1} \qquad eq.7$$

As soil characteristics were not reported in Drake *et al.* (2018), soil parameters were taken from Cowan (1965).

Model runs

To generate a range of behavior in the model, a series of values of β were investigated ranging from β=1 to β=2.5. The first three days of each model run represent a transient period during which the initial uniform soil moisture decayed to a repeating daily cycle (stationary-state) comparable to the Drake experiment. To test the effect of a reduction in the water potential for a 50% reduction in g_s (*i.e.*, $g_s\Psi_{50}$), a proxy for leaf osmotic adjustment, two additional model runs were compared with $g_s\Psi_{50}$ set to -1.33 or -2.66 MPa, and β=1 or 2, with other parameters unchanged. The soil diffusivity and β were then varied in a series of model runs to explore the general conditions for the emergence of aniso/isohydry and feed-forward behavior. Model runs and figures were coded and evaluated in Mathematica 14 (Wolfram Inc., Champaign IL, USA; Supplemental Information Notes **S2**).

Results

Recovery of intra- and inter-day patterns of transpiration under a doubling of VPD

Following a three-day initialization period, the model reproduced the diel stationary states and inter-day conservation of *E* across both treatments seen in the physical experiment (Drake *et al*., 2018; their Fig. **2**). Other behaviors could be produced for some initial conditions, including negative values (foliar uptake and hydration of the soil from the atmosphere at the dew point, not observed by Drake *et al.* (2018)) or longer-phase (multi-day) oscillations of the potential flux (data not shown). The model was judged to have converged on a solution when the total daily flux into the rooting plane reached a stable value of 0.15 +/- 0.005 (3.33%) cm day^{-1}. Root surface water potentials were sufficiently dry that no serious errors were introduced by the steady asymptotic flux boundary condition (Fig. 2b, Supplemental Information Figs. **S1-S4**), and diurnal variations in φ, *h*, and Ψ did not reach the source side of the model domain from the rooting plane, indicating the 10 cm depth chosen for *H* was sufficient to capture all time dependent soil effects (Supplementary Information Figure **S5**).

For the Control conditions of *nVPD* 1 and 1.25 transpiration closely tracked diurnal variations in potential transpiration (Fig. **2a**, **3a** blue). Doubling *nVPD* (and so β) to 2 and 2.5 respectively for

the Heat Wave treatment showed earlier peaks and feed-forward declines in *E* (*i.e.*, *E* falling as *nVPD* is still increasing) relative to the control (Fig. **2a**, **3a** red). Examination of the diurnal cycles of root and leaf water potentials shows that the loss of soil conductivity at the higher levels of β and *nVPD* of 2 and 2.5 similarly depressed root and leaf water potential to about -1.2 and -1.5 MPa (Fig. **2b, 3b** dotted and solid red lines respectively). Yet, the low-stress conditions of β=*nVPD*=1and β=*nVPD*=1.25 showed very different midday water potential depressions of -0.15 MPa (root) and -0.6 MPa (leaf), versus -0.7 and -1.2 MPa (Fig. **2b,3b** dotted and solid blue lines for root and leaf respectively). Interpreted as a response to *VPD* (Martínez-Vilalta *et al.*, 2014), the doubling from β=*nVPD*=1 to 2 produced an anisohydric shift in midday leaf water potential from -0.6 to -1.5, while the doubling from β=*nVPD*=1.25 to 2.5 showed a more isohydric pattern of -1.2 to -1.5 MPa. This shift in behavior derived from root surface drying pushing stomatal conductance into the region of steep declines near $g_s\Psi 50$, resulting in more isohydric regulation of *E* (Fig. **1c, 2c, 3c**). In the physical experiment, both Control and Heat Wave leaf water potentials fell in a similar range around -1.5 MPa (Drake *et al.*, 2018) in an apparent isohydric response to demand consistent with the model behavior for doubling *nVPD* from 1.25 to 2.5.

The above results suggest that both $g_s\Psi_{50}$ and the degree of soil drying control the transition from anisohydric to isohydric behavior. Yet, running the model for both *nVPD* 1 and 2 with $g_s\Psi_{50}$ doubled from -1.33 to -2.66 MPa (Fig. **4**) shows that in response to elevated *nVPD* the water potential at the rooting surface (Fig. **4e** vs **4b**) drops precipitously to force leaf water potential to whatever level is required to limit transpiration to the available soil flux (Fig. **4f** vs **4c**). The ultimate effect of 'osmotic adjustment' in the stomatal setpoint $g_s\Psi_{50}$ was then to steepen the feedforward behavior of the Heat Wave trees (Fig **4a** vs **4d**) and to lower the minimum leaf water potential (Fig. **4c** vs **4f**) without extracting more water out of the soil over the day.

General controls on the emergence of feed-forward and isohydric behavior

That the doubling *nVPD* from 1.25 to 2.5 showed an isohydric response of leaf water potential without the emergence of strong feed-forward declines in *E* at *nVPD* 1.25 suggests these behaviors are independent. Sensitivity analyses show that this apparent independence is true only in part (Fig. **5**). Varying β from 1 to 5 (with nominal diffusivity D_o=25.7) shows that feedforward control steepens as the imbalance of supply and demand becomes large (Fig. **5a**), while isohydry

emerges between β 1 and 2, with only a small further decline in midday leaf water potential as β grows to β=5 (Fig. **5b**). Both the emergence of feedforward and isohydry can result from increasing β. Yet, this coupled response is not seen for low values of the soil diffusivity (*i.e.,* higher clay fractions: Jury *et al.*, 1991; Koehler *et al.*, 2024; Wankmüller *et al.*, 2024)).

Lowering the nominal diffusivity in steps from 25.7 to 1 while holding β at 2.5 shows that feedforward behavior vanishes as the time scales for the soil to respond to diurnal changes in demand become longer, smoothing E over the course of the day (Fig. **5c**). The lack of any significant change in the response of midday leaf water potentials shows that isohydry is far less sensitive (Fig. **5d**). This is confirmed by a sweep of β from 1 to 2.5 at D_o=1 (Fig. **5e,f**). In the 'slow' soil D_o=1 regime, increasing β results in peak broadening instead of feedforward behavior (Fig. **5e**), while midday leaf water potentials show the same transition to isohydry as for high D_o (Fig. **5f**). Isohydry develops due to supply imbalance (β >1) alone.

How low soil diffusivity suppresses the development of feedforward behavior in response to β >1 can be understood by examining the spread between the gradients of water potential in the soil domain at the minima and maxima of *nVPD* (Fig. **6**). At β=1, E tracks potential E at both low (D_o=1; Fig. **6a**) and high (D_o=25.7; Fig. **6b**) nominal soil diffusivities, yet the soil gradients behave very differently. At the lower diffusivity, the soil is slow to respond to the diel cycle and capacitive discharge is damped and overnight relaxation is small (Fig. **6c**). At the higher nominal diffusivity, the soil response is fast and the soil gradient relaxes overnight to a large degree (Fig. **6e**). This difference is captured by the 'damping depth,' δ, the distance from the rooting plane into the soil domain that diel oscillations are expected to reach:

$$\delta = \sqrt{\frac{2\, D_o \varphi}{\tau_d}}, \qquad eq.8$$

At low nominal diffusivity, the time-invariant gradient from z=0 to z=9 cm moves the steady flux of 0.15 cm day^{-1} with no capacitive discharge (Fig. **6c,d**), while the midday excess transient flux up to the peak of 0.3 cm day^{-1} is met by capacitive discharge within the last cm. As the gradient hardly relaxes, when β is doubled to 2 it is already diverging and the total soil flux (J_m + capacitive discharge) becoming asymptotic at the root plane (compare Fig. **6c** to **6d)**. As a result the stomata are rapidly pushed toward their $g_s\Psi_{50}$ and E fails to follow potential E the more it exceeds J_m (Fig. **6a**, dashed red vs solid red lines).

For both fast and slow soils, the doubling of potential E relative to J_m spreads the net discharge of stored water over a longer period that starts earlier in the day. This leaves less dischargeable water to meet peak midday demand, leading to reduced midday E relative to β=1 (Fig. **6a**) for both high and low nominal diffusivity. Yet, at high nominal diffusivity, relaxation of the soil gradient is pronounced relative to low diffusivity as the damping depth extends below 9 cm (Fig. **6b,e**). When potential E is doubled at *nVPD* 2, this increased relaxation allows capacitive discharge to be 'pulled-forward' in the early a.m. (skewed light blue region in Fig. **6b**) to track potential E for longer before the soil gradient diverges (Fig. **6f**). The early peak then collapses in a feedforward manner as soil capacitive water release becomes exhausted. The transient asymptotic level of E then decays toward the steady flux (Fig. **6b**, red dashed line) as the soil gradient diverges to push stomata to their $g_s\Psi_{50}$ (Fig. **6f**).

Why the collapse in capacitive discharge? Water release becomes increasingly confined to a region near the rooting plane as demand increases. While at β=2 a faster soil leads to a deeper damping depth and greater overnight gradient relaxation (Fig. **6d,f**) that allows E to track potential E farther along its curve (Fig. **6a,b**), the doubling of β itself drops the damping depth by more than half (Fig. **6d** vs **6c**, **6f** vs **6e**). This decrease occurs due to the realized diffusivity's ($D_o\varphi$) dependence on the local moisture state of the soil. Evaluating δ (eq. 7) at the rooting plane (z=H) selects the lowest value of the soil diffusivity $D_o\varphi$ in the system, and it is this minimum diffusivity that controls the damping depth (dotted lines Fig. **6c,d,e,f**). As potential E increases both in the a.m. and across treatments, $D_o\varphi$ at the rooting plane decreases, and this shallowing of the damping depth constrains soil water release: the shallow drier soil increasingly feels the 'squeeze' of atmospheric demand rather than the deeper wetter soil. Diurnally increasing confinement of the gradient causes capacitive discharge to collapse, pushing stomata into feedforward regulation. This amplification of stress in the soil region nearest the rooting plane then plays an important role in creating the behavior of a 'hydraulic rope' that as the system pulls harder breaks strands rather than pulls more water (Sperry & Love, 2015).

How does the steady flux from outside the domain contribute to the above dynamics? An inward flux from deeper soil controls the total amount of water that can be transpired in a diel stationary-state: as J_m goes to zero no stationary state occurs as the total moisture of the root and soil domain declines monotonically (Cowan, 1965), and the maximum asymptotic flux *at the*

root surface has only a transient component derived from capacitive discharge. The capacitive confinement effects due to declines in $D_o\varphi$ over and within days that drive feed-forward behavior will still occur. β is not defined for this case, with the balance of atmospheric demand and capacitive soil supply entering instead into the time scale for soil moisture depletion that also controls feedforward and isohydric behavior (Tuzet *et al.*, 2003; Supplemental Information Notes S1).

Interpretation of empirical model parameters

Plotting the instantaneous diurnal values for stomatal conductance against instantaneous *nVPD* (i.e., *nVPD* level multiplied by the diurnal function) results in an apparent stomatal response to *nVPD* (Fig. **7**). Fig. **7a** shows the fit of the *VPD* sensitivity model of Oren *et al.* (1999) $g_s = g_{s,ref}$ (1- m ln[$nVPD$]) to the simulated data. Across all four experimental model runs, the bulk soil moisture at the source-edge of the model domain remained the same ($\varphi \sim 2$, $\theta \sim 0.28$, Supplemental Information Fig. **S6)**, justifying the aggregation of observations of g_s across all *nVPD* and fitting a single $g_{s,ref}$ and m. These parameters are highly sensitive to the specific level of *VPD* chosen as a reference, 3 kPa (Control trees: Drake *et al.*, 2018). Re-basing *nVPD* to the standard reference of 1 kPa results in a value for the slope m of 0.42, consistent with previous estimates for soil moisture limited systems (Oren *et al.*, 1999; Novick *et al.*, 2016a; Grossiord *et al.*, 2020). As there was considerable a.m./p.m. hystersis in the relation of g_s to *nVPD*, the reference value at *nVPD* 1 was $g_{s,ref} = 0.78$ rather than the expected 'stress-free' value of 1: nevertheless the fitted slope of 0.79 picked-out the midday values of g_s as the diurnal spread converged at peak stress.

A second empirical model of *VPD* sensitivity is that stomata adjust to conserve a steady-state balance between liquid and vapor phase transport, forcing g_s to fall as 1/*vpd* (Fig. **7b;** Oren *et al.*, 1999; Grossiord *et al.*, 2020; Mencuccini et al., 2024). For the Drake experiment, a steady mass-balance holds on average over a diel stationary-state, taking the form $g_s = g_{s,ref}/nVPD$ (Fig. **7b**; derivation in Supplemental Information Notes **S1**). Fit to the same simulated data as the log-based model, neither is preferred based on fit statistics, and both capture the peak-stress relationships between *nVPD* and g_s that are taken as representative of a system (Martínez-Vilalta *et al.*, 2014; Hochberg *et al.*, 2018; Knipfer *et al.*, 2020).

The two empirical approaches do predict contrasting behaviors of *E* that coincide with the physical experiment at different time scales (Fig. **8a,b** top panels**)**. For the log-based model the response of *E* transitions from feedback to feedforward at about 2 *nVPD*, qualitatively consistent with the diurnal development of feedforward responses in the physical experiment (Figs. **2, 3**; Drake *et al.*, 2018), and responses observed in leaf-scale gas-exchange experiments (Mott & Parkhurst, 1991). Yet the log-based model fails to reproduce the observed conservation of *E* across days (Fig. **8a**). The mass balance approach by contrast could *only* capture conservation across days, as it predicts a single value of *E* independent of diel variations in *nVPD* (Fig. **8b**).

In the full model presented here, static declines in bulk soil water potential lower the maximum stomatal conductance that would pertain at zero *E*, while non-zero *E* induces a dynamic drop in water potential that drives feed-forward stomatal behavior. The log-based model renders this partitioning between static ($g_{s,\mathrm{ref}}$) and time-dependent dynamic (m) effects as steady-state behaviors, and an apparent pathology of this model structure is that at high *VPD* the model predicts lower g_s at higher soil moisture than at low (dotted lines in Fig. **8a**). By contrast, in the mass balance model as the soil dries out falling J_m generates a more realistic sequence of curves (Fig. **8b)** that decay toward a converging response to *VPD*.

The contribution of boundary layer feed-backs to apparent stomatal VPD responses

The above discussion applies directly to the case that stomata represent the controlling resistance between plants and a well-mixed atmosphere. Yet, over time transpiration can humidify the air within and above the canopy to create a feed-back on *E* as the driving force for transpiration decays. Treating the state of the soil and *VPD* as independent variables represents a zero-coupling limit of land-atmosphere interactions that then may not pertain at the time and spatial scales of interest (McColl *et al.*, 2019; McColl & Rigden, 2020). For a fully coupled land-atmosphere system in steady-state, ETRHEQ/SFE picks out the surface conductance consistent with the observed RH of the ABL (Fig. **8c**; see Supplemental Information Notes **S1**). At high RH (low VPD) states of SFE, large reductions in initially high values of g_s are associated with small reductions in RH (increases in *VPD*). Yet in this humid limit large changes in g_s are associated with very small changes in *E* (Fig. **8C**, inset). This behavior recalls that of the thick boundary layer limit (Jarvis & McNaughton, 1986) and equilibrium evaporation (Raupach, 2001).

Limitations of the model

That the neglect of the cylindrical geometry of the soil around a root did not materially affect the results was confirmed by a comparison of the solutions for β=1 and 2 in radial and cartesian domains: in both cases for high β the potential at the root surface diverges to force stomatal closure (Supplemental Information Fig. **S6**). Similarly, the neglected possibility of a decline in plant hydraulic conductance would be expected to reduce how far root surface potentials diverge to shut stomata, but not to qualitatively change the emergence of a limiting soil flux. The steep non-linearity of the stomatal conductance function in the φ domain (Fig. **1e**) did appear to introduce numerical artifacts evident as sharp deviations from otherwise smooth curves (*e.g.*, Day 1 and 4 minimum g_s in Fig. **3c**). Such artifacts could be diagnosed by their vanishing in model runs after small changes to the initial conditions.

Discussion

Limitation of transpiration by an emergent maximum flux as a general property of the land surface

The emergence of a steady-state asymptotic flux is a general feature of passively driven flow through media in which increasing driving force feeds back negatively on the conductivity, like plant xylem (Sperry & Love, 2015) or soil (Cowan, 1965; Carminati & Javaux, 2020). While most previous work has focused on steady-states, this study shows how diurnal time-dependent declines in soil diffusivity can drive the increasing confinement of the soil gradient to near the root surface, causing the transient contribution to the maximum soil flux to decay. This decay is then transduced by the functional dependance of stomata on leaf water potential into feedforward control. Iso/anisohydric transitions emerge over longer times scales as either the quasi-steady component of the maximum soil flux declines or peak VPD stress increases. With respect to the generality of the Drake *et al.* (2018) results, the conserved transpiration rate of 1.5 mm day^{-1} obtained in the chambers was well-within the range for *Eucalyptus* forest and plantations, as well as North American temperate forest (Forrester et al, 2010; Zolfaghar 2017; Shveytser 2024). The generality of the modeled stomatal behavior is supported by the empirical parameter fits to the aggregated g_s data, and the underlying soil and stomatal water potential ‘set points’ are within the expected values for a survey of soils and17 diverse tree species (Carminati et al, 2026).

Predicting maximum steady soil fluxes at scale hinges on the availability of soil texture data (Wankmüller *et al.*, 2024), source depth (*e.g.*, a water table: Miguez-Macho & Fan, 2021) and

rooting depth (Fan *et al.*, 2017). Fan *et al.* (2017) describe how root growth follows infiltration depth; if this depth is shallower than the capillary fringe of ground water, a 'dry gap' is created between the rooting zone and deep soil moisture. For 501 taxa, Fan *et al.* (2017) found maximum rooting depth clusters between ~25 cm and 2 m, with the highest density at 1m, paired with water table depths clustered between 1 and 10 m. Meter-scale dry gaps during drought may then occur for many, if not most, woody plants. Some trees obligately produce dimorphic roots, building both a shallow root system to access nutrients and seasonally available rainfall, as well as deep roots that cross a dry gap to reach groundwater and avoid seasonal drought (Skelton *et al.*, 2021), shifting the characteristic depth of root uptake. Such deep sources need not be saturated (*i.e.*, a water table) to supply a steady maximum flux, just approximately fixed at some potential over the time scale of interest (Supplemental Information Notes S1; Fig. S4).

Successfully modeling a stationary-state with a flux of moisture from outside the root zone to a plane of root uptake implies that the root-to-shoot ratio no longer mediates soil and shoot fluxes as it does for uptake from an evenly-moist soil volume: this may be realistic when only the wettest part of the root zone matters (Dawson *et al.*, 2020). Yet, to the extent an external inward flux can be spread evenly over the total root surface area, greater rooting volume and density will damp away feedforward behavior, but not the emergence of isohydry (Supplemental Information Notes S1).

The surprising sufficiency of stomatal conductance as a function of leaf water potential

The analyses presented here demonstrate that a model of stomatal aperture as a function of a single integrative variable – water potential – is sufficient to capture both anisohydric to isohydric transitions (Knipfer *et al*., 2020; Javaux & Carminati 2021) and feedforward responses to *VPD*. This is surprising as it was the failure of leaf water potential ψ_L and g_s to follow a 1:1 relationship in response to *VPD* and soil drying over physiological time scales that motivated work on the role of chemical signaling in stomatal behavior (Turner *et al.*, 1984, 1985; Gollan *et al.*, 1985; Tardieu & Davies, 1992; McAdam & Brodribb, 2016).

One possible reason for the failure of g_s to track ψ_L is that measurements of bulk leaf water potential may not capture the water status relevant to stomata (Rockwell *et al.*, 2014; Buckley *et al.*, 2017). Measurements with fluorescing nanogel reporters of water potential point to the existence of large (up to MPa scale) gradients in water potential from leaf xylem to the

transpiring surface (Jain *et al.*, 2024b,a), which may explain why Anderegg *et al.* (2017) found that a Ball-Berry based model of stomatal conductance that included both a leaf water potential and a *VPD* sensitivity term was preferred: The bulk measure of leaf water potential may be dominated by leaf tissue that sits close to leaf xylem potential, while a *VPD* sensitivity term may capture gradients within the leaf proportional to g_s*VPD/K_m, such that there is no 'double-counting' (Liu *et al.*, 2020b). In this view, it seems relevant that in an influential series of papers demonstrating the failure of g_s to track ψ_L (Turner *et al.*, 1984, 1985; Gollan *et al.*, 1985), leaf water potential was measured by in-situ psychrometers, a technique shown to track stem xylem potential at the point of leaf insertion (Matzner & Comstock, 2001). Unsaturation in the leaf air spaces (Márquez *et al.*, 2024; Cernusak *et al.*, 2024; Diao *et al.*, 2024) could also be a factor, yet, as noted by Grossiord *et al.* (2020), this effect should be 'passed through' by parameter observations that ultimately deliver correct predictions of stomatal responses.

Biological vs physical controls on surface conductance and empirical model parameters

Mott & Parkhurst (1991) showed that stomata respond to *E* rather than directly to *VPD* or RH at the leaf surface. Yet, currently there is no complete description of the mechanisms within a leaf that are involved in feedforward and feedback type stomatal responses to *VPD* (Grossiord *et al*, 2020). The evident ability of a physical null model in this study to generate these behaviors does not mean that biology does not matter for *VPD* responses. Rather, a successful null model is useful for exposing what biological parameters are likely to matter most. With respect to the mechanistic interpretation of empirical model parameters, the model suggests that *m* and g_{ref} are responsive to different physical forcings originating from different moisture states within the same soil (rhizosphere vs bulk). While correlated across biomes (Novick *et al.*, 2016a), these parameters may be to some degree uncoupled across species by biological factors like variations in root density, hairiness and root exudation that impact the scale and degree of soil-root contact (Carminati *et al.*, 2009, 2016; Wankmüller *et al.*, 2024; Akale *et al.*, 2025). In this regard *m* may be expected to act like a biologically influenced parameter partially independent of bulk soil moisture and g_{ref}.

From the perspective of optimization models of stomatal conductance, feedforward behavior and midday closure have been interpreted as conserving a target proportionality between carbon gain and water loss (Novick *et al.*, 2016b; Anderegg *et al.*, 2017; Dewar *et al.*, 2018; Wang *et al.*,

2020; Gardner *et al*., 2023). In the null model presented here, feedforward behavior is decidedly sub-optimal as it derives from the decay of excessive rates of water loss in the a.m. The suggestion is not that stomatal behavior in no-way optimizes instantaneous water-use efficiency, rather that optimization may also occur over longer time scales through adjustments of root-to-shoot ratio, root depth, or soil-root contact that effectively decrease β and premature peaking of g_s out of phase with peak irradiance.

Stomatal responses to VPD and the control of transpiration

In the 'de-coupled limit' of a thick boundary layer at the canopy scale (Jarvis & McNaughton, 1986), large changes in stomatal aperture achieve small changes in transpiration. SFE also predicts that at high RH in the ABL large reductions in surface conductance are associated with small reductions in *E*. Changes in RH in the ABL feedback on transpiration as a change in driving force, but there is no feedback of RH on the value of the surface conductance. That SFE can explain ETRHEQ and patterns of g_s versus *VPD* from flux tower data (McColl & Rigden, 2020) suggests that at this scale apparent responses to *VPD* are not driven by physiological feed-backs of *VPD* on g_s. In the moist land surface and atmosphere limit, the important intuition that emerges is not that g_s is highly sensitive to a stress imposed by atmospheric aridity, but that g_s exerts weak control over the evaporative flux.

In the dry limit, the apparent sensitivity of g_s to *VPD* is less but the sufficiency of a theory lacking a feedback of *VPD* on g_s still pertains. While for mesic systems *VPD* responses at the daily time scale show a single curve across all soil moisture quantiles as expected by ETRHEQ/SFE (Novick *et al*., 2016a), arid systems tend to show a family of curves comparable to the response of empirical models described here (Fig. **8**). This difference may arise due to drier systems requiring longer than daily time scales to reach Surface Flux Equilibrium (SFE) (McColl & Rigden, 2020). Yet once at SFE, stomatal behavior may be as physically constrained by SFE/ETRHEQ as the formation of a soil crust. (Vargas Zeppetello *et al*., 2023). From this perspective, the critical biological plant factors contributing to the partitioning of surface latent and sensible heat fluxes are likely those that mediate root and soil contact (Carminati *et al*., 2016) and so scale the maximum flux available to the evaporative surfaces of the canopy, rather than autonomous stomatal controls.

Conclusion

The influence of *VPD* on stomatal aperture is strongly mediated by the state of the soil, and variations in apparent responses of stomatal conductance to *VPD* at constant bulk soil moisture are not necessarily under biological control. The emergence of isohydry is driven by the integrated daily balance of potential transpiration to maximum soil supply (β, in the stationary-state). Emergence of feedforward regulation E is time-dependent and driven by both supply and demand imbalance and the soil diffusivity, which is soil texture dependent. While steady-state empirical model parameters can be mapped to hydraulic mechanisms, these reduced models struggle to capture relevant responses of E. These results motivate further investigation into the physical and biological factors controlling the surface conductance coupling plant canopies to the atmospheric boundary layer.

Acknowledgements

Abraham Stroock, Guido Salvucci, Kaighin McColl, Daniel Short Gianotti and N.M. Holbrook provided valuable feedback and discussion. This work was supported by NSF-MRSEC DMR-2011754.

Competing interests

None declared

Data availability

No new data were generated in this study, and all simulated data are available by evaluating the code given in Supplemental Information Notes **S2**.

Figure legends

Figure **1**. Minimal hydraulic model of the soil-plant-atmosphere continuum. **a** The last few centimeters of the distance L from the water table to rooting depth forms the modeled soil domain height H, bounded at the lower surface by a maximum flux from the water table J_m, and at the upper surface by a variable root uptake flux equivalent to transpiration E, as driven by the product of a diurnal demand function $f(t)$ (in **b**) and $nVPD$. **c** Dimensionless stomatal conductance g_s as a function of leaf water potential Ψ [MPa], with the $g_s\Psi_{50}$ for a 50% decline in stomatal conductance set at -1.33 MPa (dotted lines). In the modeled domain **d**, water content θ depends on soil hydraulic conductivity $K(h)$ [cm day^{-1}] and the gradient in matric potential h

[cm]. **e** Transformation of the water content, matric and water potentials to the potential flux domain [φ, cm^2 day^{-1}] linearizes the governing equation, but results in an extremely steep function for g_s that hinders numerical solution.

Figure **2**. Emergence of feedforward and counter-factual anisohydric behavior in the model for the heat wave experiment in Drake *et al.* (2018) for normalized vapor pressure deficit (*nVPD*) levels of 1 (Control, blue lines) and 2 (Heat Wave, red lines). The first three days (shaded) represent a 'dry-down' from a SMC θ = 0.25 used to initialize the model to a four-day quasi-steady diurnal cycle comparable to the physical experiment. (**a**) Diurnal cycles of *E* for the Heat Wave peak earlier and show feedforward declines relative to the control that conserves total daily *E* (inset bar chart). (**b**) Diurnal cycles of root (dashed) and leaf (solid) water potential Ψ show an anisohydric response across *nVPD* levels as leaf Ψ more than doubles in magnitude. (**c**) Diurnal variations in g_s show minor g_s limitation at *nVPD* 1 while at *nVPD* 2 g_s is forced to below 50% at midday: inset bar chart of integrated total g_s over four days shows that *A* and *E* become decoupled at high *nVPD*.

Figure **3**. Emergence of feedforward and isohydric behavior as observed in the heat wave experiment in Drake *et al*. (2018) for normalized vapor pressure deficit (*nVPD)* levels of 1.25 (Control, blue lines) and 2.5 (Heat Wave, red lines). The first three days (shaded) represent a 'dry-down' from a SMC of θ = 0.25 used to initialize the model to a four-day stationary diurnal cycle comparable to the physical experiment. (**a**) Diurnal cycles of *E* for the Heat Wave peak earlier and show feedforward declines relative to the control that conserve total daily *E* (inset bar chart). (**b**) Diurnal variations in root (dashed) and leaf (solid) water potential create a near 'isohydric response' of Ψ_{leaf} to *nVPD*. (**c**) Diurnal variations in g_s show stomatal limitation at midday at both *nVPD* levels: inset bar chart of total integrated g_s shows *A* and *E* are more decoupled at higher *nVPD*.

Figure **4**. Effect of doubling $g_s\Psi_{50}$ ('osmotic adjustment') from -1.33 MPa (**a**,**b**,**c**) to -2.66 MPa (**d**,**e**,**f**) with *nVPD* 1 (blue) and *nVPD* 2 (red). **a,d** Diel course of transpiration in the stationary state: maintaining higher g_s to lower Ψ stretches the a.m. peak, but *E* for both setpoints converges rapidly once stomata start to constrain the water flux. **b**,**e** Gradients of water potential through the soil domain at the nocturnal maximum and diurnal minimum of *nVPD*: the space between the two lines (light blue) for each level of *nVPD* shows the region of the domain subject to daily

fluctuations in water content, which remain confined to near the rooting plane (z=10 cm). **c**,**f** Diel course of soil (dashed) and leaf (solid) water potential; at *nVPD* 2 shifting stomatal closure to a value twice as negative allows leaf water potential to fall to values almost twice as dry but fails to pull a larger midday or total daily water flux from the soil (**a**,**d**).

Figure **5.** Emergence of feedforward control of transpiration E and isohydry in the soil-plant system. E (a,c,e) is normalized to the flux recharging the soil domain J_m, and water potential (b,d,f) is normalized to the value at 50% stomatal closure. **a** A parametric sweep across β equal to 1 (blue solid), 1.5 (blue dashed), 2 (red dashed) and 5 (red solid) shows the emergence of feedforward control at high D_o=25.7. **b** Diel course of leaf (solid) and root (dashed) water potentials show a transition from anisohydric to isohydric for the same simulations as in **a** as the drying root surface forces stomata to shut. **c** Decay of feedforward control at β=2.5 as D_o falls from 25.7 (red) to 15 (blue), 5 (black dashed) and 1 (black solid). **d** Diel course of leaf (solid) and root (dashed) water potentials for the simulations in **c** showing no change in the pattern of midday leaf water potentials but greater relaxation at pre-dawn as D_o falls. **e** Parametric sweep across β levels 1 (blue solid), 1.5 (blue dashed), 2 (red dashed) and 2.5 (red solid) showing that at D_o=1 peak broadening replaces the emergence of feedforward control due as β increases. **f** The emergence of isohydry at D_o=1 follows the same pattern as at D_o=25.7.

Figure **6**. Diel course of potential transpiration (solid) and actual transpiration E (dashed) normalized to the inward soil flux J_m at β=1 (blue) and β =2 (red) and D_o =1 (**a**) and 25.7 (**b**); light blue shading indicates periods of net recharge (below E= J_m) and discharge (above E= J_m) with respect to the β=2 case, with the heights proportional to the magnitude of the recharge/discharge flux at that instant. **c**,**d**,**e**,**f**: Gradients in soil water potential relative to the leaf water potential for 50% stomatal closure at the daily min and max of E; the light blue region shows the location and potential range for transient release of water (note the difference in potential scales), relative to the damping depth δ. Panels **c,d** correspond to **a,** and **e,f** to **b.** Note that position in the soil domain z and damping depth δ are expressed relative to the domain size H.

Figure **7**. Fits of simulated diurnal values (hysteretic loops) of stomatal conductance for two contrasting models of stomatal sensitivity to *VPD.* Data are for all four modeled *nVPD* levels (cyan 1, green 1.25, red 2, blue 2.5); black solid lines show the fit and dashed lines the 99% CI. **a**

Log-based model: $g_s = g_{s,ref}$ (1- m ln[$nVPD$]), $g_{s,ref}$ =0.78, m = 0.79, adjR^2 = 0.96. **b** Mass-balance based model: $g_s = g_{s,ref} / nVPD$, $g_{s,ref}$ =0.78, adjR^2 = 0.96.

Figure **8**. A comparison of the normalized conductance extinction curves ($g_s/g_{s,ref}$) and transpiration responses (E/E_{ref}) for three simplified models of stomatal responses to soil drying and atmospheric aridity, with 1 kPa as the reference state for *nVPD*. **a** Based on the behavior of the dry sites in figure 2 of Novick *et al.* (2016), as the soil dries in the model $g_s/g_{s,ref} = a$ (1- m ln[$nVPD$]) the intercept a falls from 1 at $nVPD$ =1 to 0.2 while the slope m falls from 0.6 to 0.2. Note that the curves representing *nVPD* responses at higher soil moisture are predicted to cross (at the transition from solid to dashed) the curves for lower soil moisture. **b** For the mass balance model $g_s/g_{s,ref} = (J_m / J_{m,ref})$ $(1 / nVPD)$, $J_m / J_{m,ref}$ falls from 1 to 0.2 to simulate a falling maximum flux as the soil dries. **c** Under the condition of Surface Flux Equilibrium (SFE), the atmospheric boundary layer approaches a constant RH (and potential *nVPD*) at all heights; responses are shown for air temperatures at two meters above the canopy of 280, 300 and 320 K.

References

Akale A, Abdalla M, Koehler T, Sauer AM, Diamantopoulos E, Ahmed MA. **2025**. Root mucilage enhances plant water use under combined soil and atmospheric drought. *Annals of Botany* **136**: 1131-1142.

Anderegg WRL, Wolf A, Arango-Velez A, Choat B, Chmura DJ, Jansen S, Kolb T, Li S, Meinzer F, Pita P, *et al.* 2017. Plant water potential improves prediction of empirical stomatal models. *PLoS ONE* **12**: 0185481.

Attia Z, Domec JC, Oren R, Way DA, Moshelion M. **2015**. Growth and physiological responses of isohydric and anisohydric poplars to drought. *Journal of Experimental Botany* **66**: 4373–4381.

Berg A, Sheffield J. **2018**. Climate Change and Drought: the Soil Moisture Perspective. *Current Climate Change Reports* **4**: 180–191.

Binks O, Cernusak LA, Liddell M, Bradford M, Coughlin I, Carle H, Bryant C, Dunn E, Oliveira R, Mencuccini M, *et al.* 2022. Forest system hydraulic conductance: partitioning tree and soil components. *New Phytologist* **233**: 1667–1681.

Brodribb TJ, McAdam SAM. **2011**. Passive origins of stomatal control in vascular plants. *Science* **331**: 582–585.

Buckley TN. **2005**. The control of stomata by water balance. *New Phytologist* **168**: 275–292.

Buckley TN. **2019**. How do stomata respond to water status? *New Phytologist* **224**: 21–36.

Buckley TN, John GP, Scoffoni C, Sack L. **2017**. The sites of evaporation within leaves. *Plant Physiology* **173**: 1763–1782.

Carminati A, Javaux M. **2020**. Soil Rather Than Xylem Vulnerability Controls Stomatal Response to Drought. *Trends in Plant Science* **25**: 868–880.

Carminati A, Javaux M, Wankmüller FJP, Brodribb TJ. 2026. Soils drive convergence in the regulation of vascular tension land plants. *Science* **391**: 6784.

Carminati A, Vetterlein D, Weller U, Vogel H-J, Oswald SE. **2009**. When Roots Lose Contact. *Vadose Zone Journal* **8**: 805–809.

Carminati A, Zarebanadkouki M, Kroener E, Ahmed MA, Holz M. **2016**. Biophysical rhizosphere processes affecting root water uptake. *Annals of Botany* **118**: 561–571.

Cernusak LA, Wong SC, Stuart-Williams H, Márquez DA, Pontarin N, Farquhar GD. **2024**. Unsaturation in the air spaces of leaves and its implications. *Plant Cell and Environment*.

Cowan IR. **1965**. Transport of Water in the Soil-Plant-Atmosphere System. *Journal of Applied Ecology* **2**: 221–239.

Cowan IR, Troughton GH. **1971**. The Relative Role of Stomata in Transpiration and Assimilation. *Planta* **97**: 325–336.

Dawson TE, Hahm WJ, Crutchfield-Peters K. **2020**. Digging deeper: what the critical zone perspective adds to the study of plant ecophysiology. *New Phytologist* **226**: 666–671.

Dewar R, Mauranen A, Mäkelä A, Hölttä T, Medlyn B, Vesala T. **2018**. New insights into the covariation of stomatal, mesophyll and hydraulic conductances from optimization models incorporating nonstomatal limitations to photosynthesis. *New Phytologist* **217**: 571–585.

Diao H, Cernusak LA, Saurer M, Gessler A, Siegwolf RTW, Lehmann MM. **2024**. Dry inside: progressive unsaturation within leaves with increasing vapour pressure deficit affects estimation of key leaf gas exchange parameters. *New Phytologist* **244**: 1275–1287.

Drake JE, Tjoelker MG, Vårhammar A, Medlyn BE, Reich PB, Leigh A, Pfautsch S, Blackman CJ, López R, Aspinwall MJ, *et al.* 2018. Trees tolerate an extreme heatwave via sustained transpirational cooling and increased leaf thermal tolerance. *Global Change Biology* **24**: 2390–2402.

Fan Y, Miguez-Macho G, Jobbágy EG, Jackson RB, Otero-Casal C. **2017**. Hydrologic regulation of plant rooting depth. *Proceedings of the National Academy of Sciences of the United States of America* **114**: 10572–10577.

Feng X, Ackerly DD, Dawson TE, Manzoni S, McLaughlin B, Skelton RP, Vico G, Weitz AP, Thompson SE. **2019**. Beyond isohydricity: The role of environmental variability in determining plant drought responses. *Plant Cell and Environment* **42**: 1104–1111.

Franks PJ, Cowan IR, Farquhar GD. **1997**. The apparent feedforward response of stomata to air vapour pressure deficit: Information revealed by different experimental procedures with two rainforest trees. *Plant, Cell and Environment* **20**: 142–145.

Franks PJ, & Farquhar GD. 1999. A relationship between humidity response, growth form and photosynthetic operating point in C3 plants. *Plant, Cell and Environment* **22**: 1337–1349.

Franks PJ, Farquhar GD. **2007**. The mechanical diversity of stomata and its significance in gas-exchange control. *Plant Physiology* **143**: 78–87.

Forrester DI, Collopy JJ, Morris JD. 2010. Transpiration along an age series of Eucalyptus globulus plantations in southeastern Australia. *Forest Ecology and Management* **259**: 1754-1760.

Gardner W. **1958**. Some steady-state solutions of the unsaturated flow equation with application to evaporation from a water table. *Soil Science* **85**: 228–232.

Gardner W, Fireman M. **1958**. Laboratory studies of evaporation from soil columns in the presence of a water table. *Soil Science* **85**: 244–249.

Gardner A, Jiang M, Ellsworth DS, MacKenzie AR, Pritchard J, Bader MKF, Barton CVM, Bernacchi C, Calfapietra C, Crous KY, *et al.* 2023. Optimal stomatal theory predicts CO2 responses of stomatal conductance in both gymnosperm and angiosperm trees. *New Phytologist* **237**: 1229–1241.

Gollan T, Turner NC, Schulze E-D. **1985**. The responses of stomata and leaf gas exchange to vapour pressure deficits and soil water content III. In the sclerophyllous woody species Nerium oleander. *Oecologia* **65**: 356–362.

Grossiord C, Buckley TN, Cernusak LA, Novick KA, Poulter B, Siegwolf RTW, Sperry JS, McDowell NG. **2020**. Plant responses to rising vapor pressure deficit. *New Phytologist* **226**: 1550–1566.

Hochberg U, Windt CW, Ponomarenko A, Zhang Y-J, Gersony J, Rockwell FE, Holbrook NM. **2017.** Stomatal closure, basal leaf embolism, and shedding protect the hydraulic integrity of grape stems. *Plant Physiology* **174**: 764-775.

Hochberg U, Rockwell FE, Holbrook NM, Cochard H. **2018**. Iso/Anisohydry: A Plant–Environment Interaction Rather Than a Simple Hydraulic Trait. *Trends in Plant Science* **23**: 112–120.

Van Den Honert TH. **1948**. Water transport in plants as a catenary process. *Discussions of the Faraday Society* **3**: 146–153.

Hunt, Jr. ER, Qu JJ, Hao X, Wang L. **2009**. Remote sensing of canopy water content: scaling from leaf data to MODIS. In: Remote Sensing and Modeling of Ecosystems for Sustainability VI. SPIE, 745409.

Jain P, Huber AE, Rockwell FE, Sen S, Holbrook NM, Stroock AD. **2024a**. Localized measurements of water potential reveal large loss of conductance in living tissues of maize leaves. *Plant Physiology* **194**: 2288–2300.

Jain P, Huber AE, Rockwell FE, Sen S, Holbrook NM, Stroock AD. **2024b**. New approaches to dissect leaf hydraulics reveal large gradients in living tissues of tomato leaves. *New Phytologist* **242**: 453–465.

Jarvis P, McNaughton K. **1986**. Stomatal control of transpiration: Scaling up from leaf to region. In: MacFadyen A, Ford E, eds. Advances in Ecological Research. London: Academic Press, 1–45.

Javaux M, Carminati A. **2021**. Soil hydraulics affect the degree of isohydricity. *Plant Physiology* **186**: 1378–1381.

Jezek M, Blatt MR. **2017**. The membrane transport system of the guard cell and its integration for stomatal dynamics. *Plant Physiology* **174**: 487–519.

Jezek M, Hills A, Blatt MR, Lew VL. **2019**. A constraint–relaxation–recovery mechanism for stomatal dynamics. *Plant Cell and Environment* **42**: 2399–2410.

Jury WA, Gardner WR, Gardner WH. **1991**. *Soil Physics*. New York: Wiley.

Knipfer T, Bambach N, Isabel Hernandez M, Bartlett MK, Sinclair G, Duong F, Kluepfel DA, McElrone AJ. **2020**. Predicting stomatal closure and turgor loss in woody plants using predawn and midday water potential. *Plant Physiology* **184**: 881–894.

Koehler T, Botezatu Á, Murugesan T, Kaliamoorthy S, Kholová J, Sadok W, Ahmed MA, Carminati A. **2024**. The transpiration rate sensitivity to increasing evaporative demand differs between soil textures, even in wet soil. *Plant Stress* **12**.

Konings AG, Gentine P. **2017**. Global variations in ecosystem-scale isohydricity. *Global Change Biology* **23**: 891–905.

Levin AD, Williams LE, Matthews MA. **2019**. A continuum of stomatal responses to water deficits among 17 wine grape cultivars (Vitis vinifera). *Functional Plant Biology* **47**: 11–25.

Liu L, Gudmundsson L, Hauser M, Qin D, Li S, Seneviratne SI. **2020a**. Soil moisture dominates dryness stress on ecosystem production globally. *Nature Communications* **11**: 4892.

Liu Y, Kumar M, Katul GG, Feng X, Konings AG. **2020b**. Plant hydraulics accentuates the effect of atmospheric moisture stress on transpiration. *Nature Climate Change* **10**: 691–695.

Manandhar A, Rimer IM, Soares Pereira T, Pichaco J, Rockwell FE, McAdam SAM. **2024**. Dynamic soil hydraulic resistance regulates stomata. *New Phytologist* **244**: 147–158.

Márquez DA, Wong SC, Stuart-Williams H, Cernusak LA, Farquhar GD. **2024**. Mesophyll airspace unsaturation drives C4 plant success under vapor pressure deficit stress. *Proceedings of the National Academy of Sciences of the United States of America* **121**: e2402233121.

Martínez-Vilalta J, Garcia-Forner N. **2017**. Water potential regulation, stomatal behaviour and hydraulic transport under drought: deconstructing the iso/anisohydric concept. *Plant Cell and Environment* **40**: 962–976.

Martínez-Vilalta J, Poyatos R, Aguadé D, Retana J, Mencuccini M. **2014**. A new look at water transport regulation in plants. *New Phytologist* **204**: 105–115.

Matusick G, Ruthrof KX, Kala J, Brouwers NC, Breshears DD, Hardy GESJ. **2018**. Chronic historical drought legacy exacerbates tree mortality and crown dieback during acute heatwave-compounded drought. *Environmental Research Letters* **13**: 095002.

Matzner S, Comstock J. **2001**. The temperature dependence of shoot hydraulic resistance: Implications for stomatal behavior and hydraulic limitation. *Plant, Cell and Environment* **24**: 1299–1307.

McAdam SAM, Brodribb TJ. **2016**. Linking turgor with ABA biosynthesis: Implications for stomatal responses to vapor pressure deficit across land plants. *Plant Physiology* **171**: 2008–2016.

McColl KA, Rigden AJ. **2020**. Emergent Simplicity of Continental Evapotranspiration. *Geophysical Research Letters* **47**. **https://doi.org/10.1029/2020GL087101**

McColl KA, Salvucci GD, Gentine P. **2019**. Surface Flux Equilibrium Theory Explains an Empirical Estimate of Water-Limited Daily Evapotranspiration. *Journal of Advances in Modeling Earth Systems* **11**: 2036–2049.

McColl KA, Tang LI. **2024**. An Analytic Theory of Near-Surface Relative Humidity over Land. *Journal of Climate* **37**: 1213–1230.

Mencuccini M, Anderegg WRL, Binks O, Knipfer T, Konings AG, Novick K, Poyatos R, Martínez-Vilalta J. **2024**. A new empirical framework to quantify the hydraulic effects of soil and atmospheric drivers on plant water status. *Global Change Biology* **30**: 17222.

Messinger SM, Buckley TN, Mott KA. **2006**. Evidence for involvement of photosynthetic processes in the stomatal response to CO2. *Plant Physiology* **140**: 771–778.

Miguez-Macho G, Fan Y. **2021**. Spatiotemporal origin of soil water taken up by vegetation. *Nature* **598**: 624–628.

Mitchell PJ, O'Grady AP, Hayes KR, Pinkard EA. **2014**. Exposure of trees to drought-induced die-off is defined by a common climatic threshold across different vegetation types. *Ecology and Evolution* **4**: 1088–1101.

Mott KA, Parkhurst DF. **1991**. Stomatal responses to humidity in air and helox. *Plant, Cell & Environment* **14**: 509–515.

Mrad A, Sevanto S, Domec JC, Liu Y, Nakad M, Katul G. **2019**. A dynamic optimality Principle for water use strategies explains isohydric to anisohydric plant responses to drought. *Frontiers in Forests and Global Change* **2**: 462736-19.

Novick KA, Ficklin DL, Grossiord C, Konings AG, Martínez-Vilalta J, Sadok W, Trugman AT, Williams AP, Wright AJ, Abatzoglou JT, *et al.* 2024. The impacts of rising vapour pressure deficit in natural and managed ecosystems. *Plant Cell and Environment* **47**: 3561–3589.

Novick KA, Ficklin DL, Stoy PC, Williams CA, Bohrer G, Oishi AC, Papuga SA, Blanken PD, Noormets A, Sulman BN, *et al.* 2016a. The increasing importance of atmospheric demand for ecosystem water and carbon fluxes. *Nature Climate Change* **6**: 1023–1027.

Novick KA, Konings AG, Gentine P. **2019**. Beyond soil water potential: An expanded view on isohydricity including land–atmosphere interactions and phenology. *Plant Cell and Environment* **42**: 1802–1815.

Novick KA, Miniat CF, Vose JM. **2016b**. Drought limitations to leaf-level gas exchange: Results from a model linking stomatal optimization and cohesion-tension theory. *Plant Cell and Environment* **39**: 583–596.

Oren R, Sperry JS, Katul GG, Pataki DE, Ewers BE, Phillips N, Schäfer KVR. **1999**. Survey and synthesis of intra- and interspecific variation in stomatal sensitivity to vapour pressure deficit. *Plant, Cell and Environment* **22**: 1515–1526.

Philip JR. **1966**. Plant water relations: some physical aspects. *Annual Review of Plant Biology* **17**: 245–268.

Raupach MR. **2001**. Combination theory and equilibrium evaporation. *Quarterly Journal of the Royal Meteorological Society* **127**: 1149–1181.

Rigden AJ, Salvucci GD. **2015**. Evapotranspiration based on equilibrated relative humidity (ETRHEQ): Evaluation over the continental U.S. *Water Resources Research* **51**: 2951–2973.

Rockwell FE, Holbrook NM, Stroock AD. **2014**. The competition between liquid and vapor transport in transpiring leaves. *Plant Physiology* **164**: 1741–1758.

Roderick ML, Greve P, Farquhar GD. **2015**. On the assessment of aridity with changes in atmospheric CO2. *Water Resources Research* **51**: 5450–5463.

Rodriguez-Dominguez CM, Brodribb TJ. **2020**. Declining root water transport drives stomatal closure in olive under moderate water stress. *New Phytologist* **225**: 126–134.

Salvucci GD, Gentine P. **2013**. Emergent relation between surface vapor conductance and relative humidity profiles yields evaporation rates from weather data. *Proceedings of the National Academy of Sciences of the United States of America* **110**: 6287–6291.

Schroeder JI, Allen GJ, Hugouvieux V, Kwak JM, Waner D. **2001**. Guard Cell Signal Transduction. *Annu. Rev. Plant Physiol. Plant Mol. Biol* **52**: 627–58.

Shiklomanov I. **1993**. World Freshwater Resources. In: Gleick PH, ed. Water in Crisis: A Guide to the World's Freshwater Resources. New York: Oxford University Press.

Shveytser V, Stoy PC, Butterworth B, Wiesner S, Skaggs TH, Murphy B, Wutzler T, El-Madany TS, Desai AR. 2024. Evaporation and transpiration from multiple proximal forests and wetlands. *Water Resources and Research* **60**: e2022WR033757.

Simonneau T, Tardieu F. **1998**. Variability among species of stomatal control under fluctuating soil water status and evaporative demand: modelling isohydric and anisohydric behaviours. *Journal of Experimental Botany* **49**: 419–432.

Skelton RP, Anderegg LDL, Diaz J, Kling MM, Papper P, Lamarque LJ, Delzon S, Dawson TE, Ackerly DD. **2021**. Evolutionary relationships between drought-related traits and climate shape large hydraulic safety margins in western North American oaks. *Proceedings of the National Academy of Sciences of the United States of America* **118**:1-9.

Sloan BP, Thompson SE, Feng X. **2021**. Plant hydraulic transport controls transpiration sensitivity to soil water stress. *Hydrology and Earth System Sciences* **25**: 4259–4274.

Sperry JS, Love DM. **2015**. What plant hydraulics can tell us about responses to climate-change droughts. *New Phytologist* **207**: 14–27.

Tardieu F, Davies WJ. **1992**. Stomatal response to abscisic acid is a function of current plant water status. *Plant Physiology* **98**: 540–545.

Tardieu F, Simonneau T. **1998**. Variability among species of stomatal control under fluctuating soil water status and evaporative demand: modelling isohydric and anisohydric behaviours. *Journal of Experimental Botany* **49**: 419–432.

Turner NC, Schulze E-D, Gollan T. **1984**. The responses of stomata and leaf gas exchange to vapour pressure deficits and soil water content I. Species comparisons at high soil water contents. *Oecologia* **63**: 338–342.

Turner NC, Schulze E-D, Gollan T. **1985**. The responses of stomata and leaf gas exchange to vapour pressure deficits and soil water content II. In the mesophytic herbaceous species Helianthus annuus. *Oecologia* **65**: 348.

Tuzet A, Perrier A, Leuning R. **2003**. A coupled model of stomatal conductance, photosynthesis and transpiration. *Plant, Cell and Environment* **26**: 1097–1116.

Vargas Zeppetello LR, McColl KA, Bernau JA, Bowen BB, Tang LI, Holbrook NM, Gentine P, Huybers P. **2023**. Apparent surface conductance sensitivity to vapour pressure deficit in the absence of plants. *Nature Water* **1**: 941–951.

Wang Y, Sperry JS, Anderegg WRL, Venturas MD, Trugman AT. **2020**. A theoretical and empirical assessment of stomatal optimization modeling. *New Phytologist* **227**: 311–325.

Wankmüller FJP, Carminati A. **2022**. Stomatal regulation prevents plants from critical water potentials during drought: Result of a model linking soil–plant hydraulics to abscisic acid dynamics. *Ecohydrology* **15**: 2386.

Wankmüller FJP, Delval L, Lehmann P, Baur MJ, Cecere A, Wolf S, Or D, Javaux M, Carminati A. **2024**. Global influence of soil texture on ecosystem water limitation. *Nature* **635**: 631–638.

Wu G, Guan K, Li Y, Novick KA, Feng X, McDowell NG, Konings AG, Thompson SE, Kimball JS, De Kauwe MG, *et al.* 2021. Interannual variability of ecosystem iso/anisohydry is regulated by environmental dryness. *New Phytologist* **229**: 2562–2575.

Zolfaghar S, Villalobos-Vega R, Zeppel M, Cleverly J, Rumman R, Hingee M, Boulain N, Li Z, Eamus D. 2017. Transpiration of Eucalyptus woodlands across a natural gradient of depth-to-groundwater. *Tree Physiology* **37**: 961-975.

Supplemental Information

Notes **S1**. Discussion and derivation of governing equations and boundary conditions.

Notes **S2**. Computer code for model runs and figures.

Figure **S1**. Maximum soil fluxes for fine sandy loam and clay soils.

Figure **S2.** Maximum soil flux for the light clay soil used in the model.

Figure **S3**. Supply curve for a clay soil as the rooting plane dries.

Figure **S4**. Supply curves for unsaturated soil moisture sources.

Figure **S5**. Evolution of the potential flux φ for all modeled levels of *nVPD*.

Figure **S6**. Comparison of cylindrical and cartesian soil and root domain solutions.

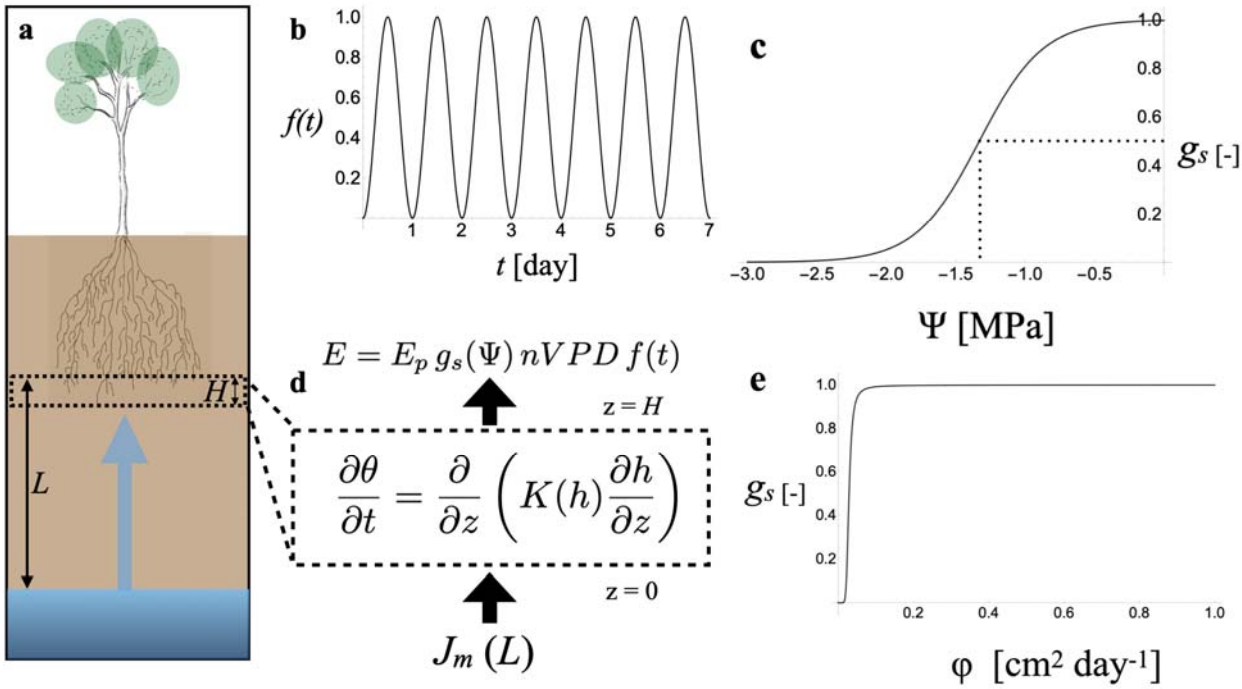

Figure **1**. Minimal hydraulic model of the soil-plant-atmosphere continuum. **a** The last ten centimeters of the distance *L* from the water table to rooting depth forms the modeled soil domain, bounded at the lower surface by a maximum flux from the water table J_m, and at the upper surface by a variable root uptake flux equivalent to transpiration *E*, as driven by the product of a diurnal demand function *f(t)* (in **b**) and *nVPD*. **c** Dimensionless stomatal conductance g_s as a function of leaf water potential Ψ [MPa], with the $g_s\Psi 50$ for a 50% decline in stomatal conductance set at -1.33 MPa (dotted lines). In the modeled domain **d**, water content θ depends on soil hydraulic conductivity *K(h)* [cm day^{-1}] and the gradient in matric potential *h* [cm]. **e** Transformation of the water content, matric and water potentials to the potential flux domain [φ, cm^2 day^{-1}] linearizes the governing equation, but results in an extremely steep function for g_s that hinders numerical solution.

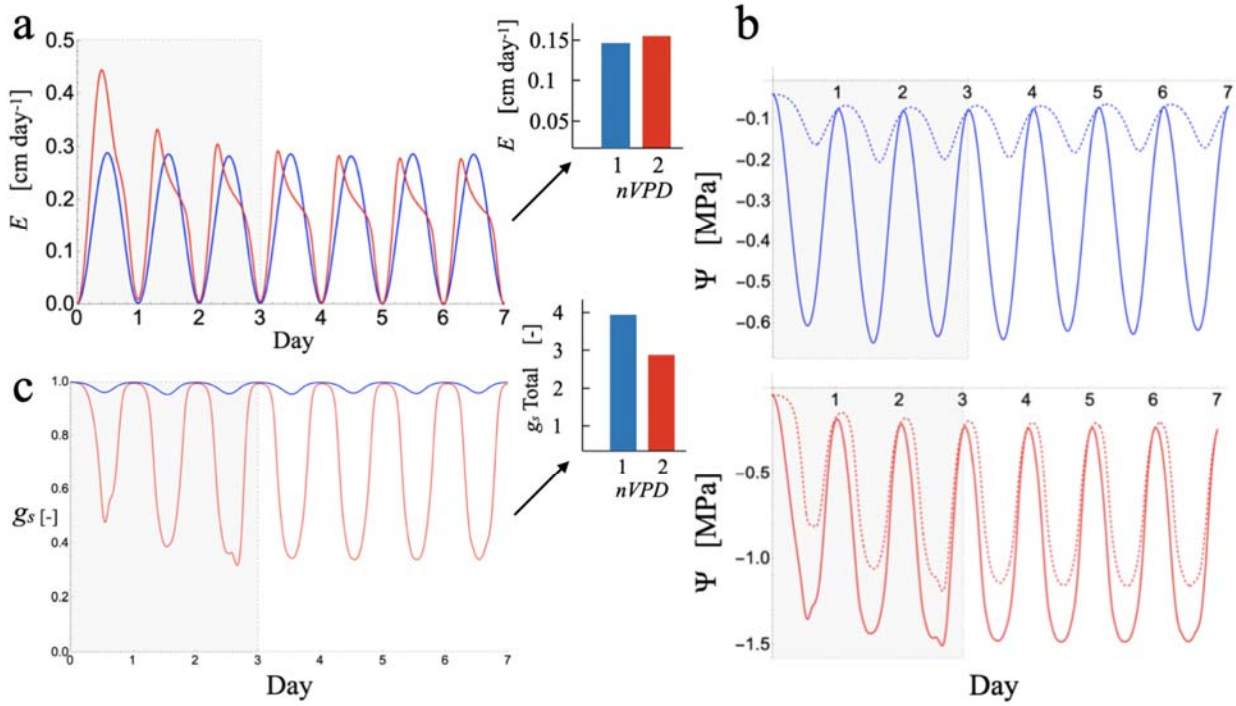

Figure **2**. Emergence of feedforward and counter-factual anisohydric behavior in the model for the heat wave experiment in Drake *et al.* (2018) for normalized vapor pressure deficit (*nVPD*) levels of 1 (Control, blue lines) and 2 (Heat Wave, red lines). The first three days (shaded) represent a 'dry-down' from a SMC θ = 0.25 used to initialize the model to a four-day quasi-steady diurnal cycle comparable to the physical experiment. (**a**) Diurnal cycles of *E* for the Heat Wave peak earlier and show feed-forward declines relative to the control that conserves total daily *E* (inset bar chart). (**b**) Diurnal cycles of root (dashed) and leaf (solid) water potential Ψ show an anisohydric response across *nVPD* levels as leaf Ψ more than doubles in magnitude. (**c**) Diurnal variations in g_s show minor g_s limitation at *nVPD* 1 while at *nVPD* 2 g_s is forced to below 50% at midday: inset bar chart of integrated total g_s over four days shows that *A* and *E* become decoupled at high *nVPD*.

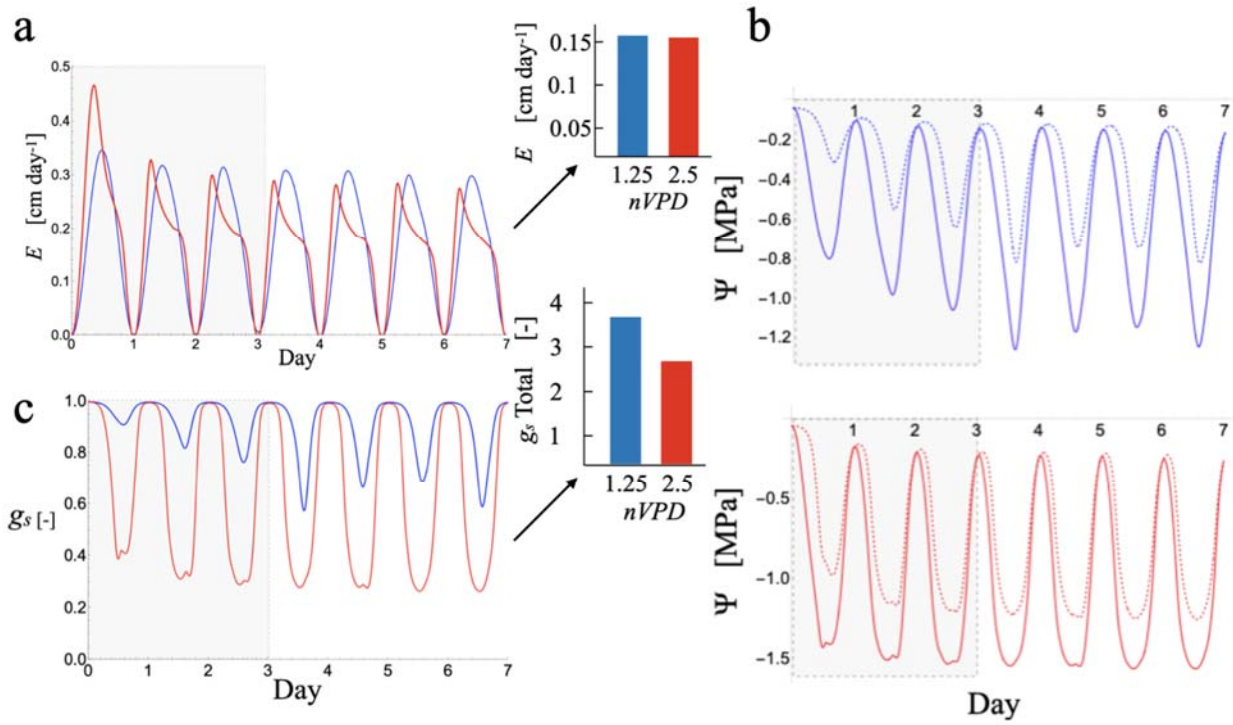

Figure **3**. Emergence of feedforward and isohydric behavior as observed in the heat wave experiment in Drake *et al.* (2018) for normalized vapor pressure deficit (*nVPD)* levels of 1.25 (Control, blue lines) and 2.5 (Heat Wave, red lines). The first three days (shaded) represent a 'dry-down' from a SMC of $\theta = 0.25$ used to initialize the model to a four-day stationary diurnal cycle comparable to the physical experiment. (**a**) Diurnal cycles of E for the Heat Wave peak earlier and show feedforward declines relative to the control that conserve total daily E (inset bar chart). (**b**) Diurnal variations in root (dashed) and leaf (solid) water potential create a near 'isohydric response' of Ψ_{leaf} to *nVPD*. (**c**) Diurnal variations in g_s show stomatal limitation at midday at both *nVPD* levels: inset bar chart of total integrated g_s shows A and E are more decoupled at higher *nVPD*.

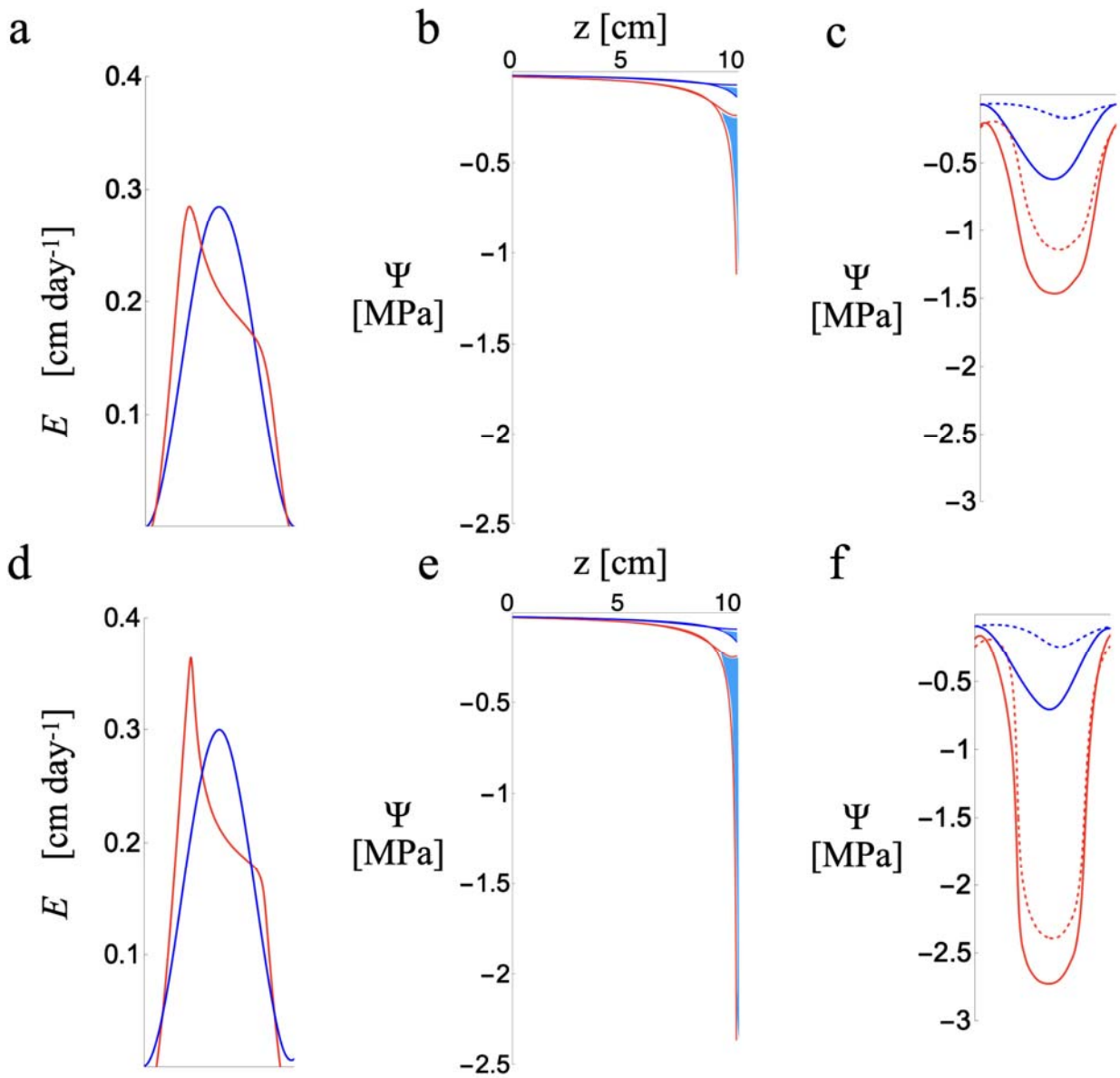

Figure **4**. Effect of doubling $g_s\Psi 50$ ('osmotic adjustment') from -1.33 MPa (**a**,**b**,**c**) to -2.66 MPa (**d**,**e**,**f**) with *nVPD* 1 (blue) and *nVPD* 2 (red). **a,d** Diel course of transpiration in the stationary state: maintaining higher g_s to lower Ψ stretches the a.m. peak, but *E* for both setpoints converges rapidly once stomata start to constrain the water flux. **b**,**e** Gradients of water potential through the soil domain at the nocturnal maximum and diurnal minimum of *nVPD*: the space between the two lines (light blue) for each level of *nVPD* shows the region of the domain subject to daily fluctuations in water content, which remain confined to near the rooting plane (z=10 cm). **c**,**f** Diel course of soil (dashed) and leaf (solid) water potential; at *nVPD* 2 shifting stomatal closure to a value twice as negative allows leaf water potential to fall to values almost twice as dry but fails to pull a larger midday or total daily water flux from the soil (**a**,**d**).

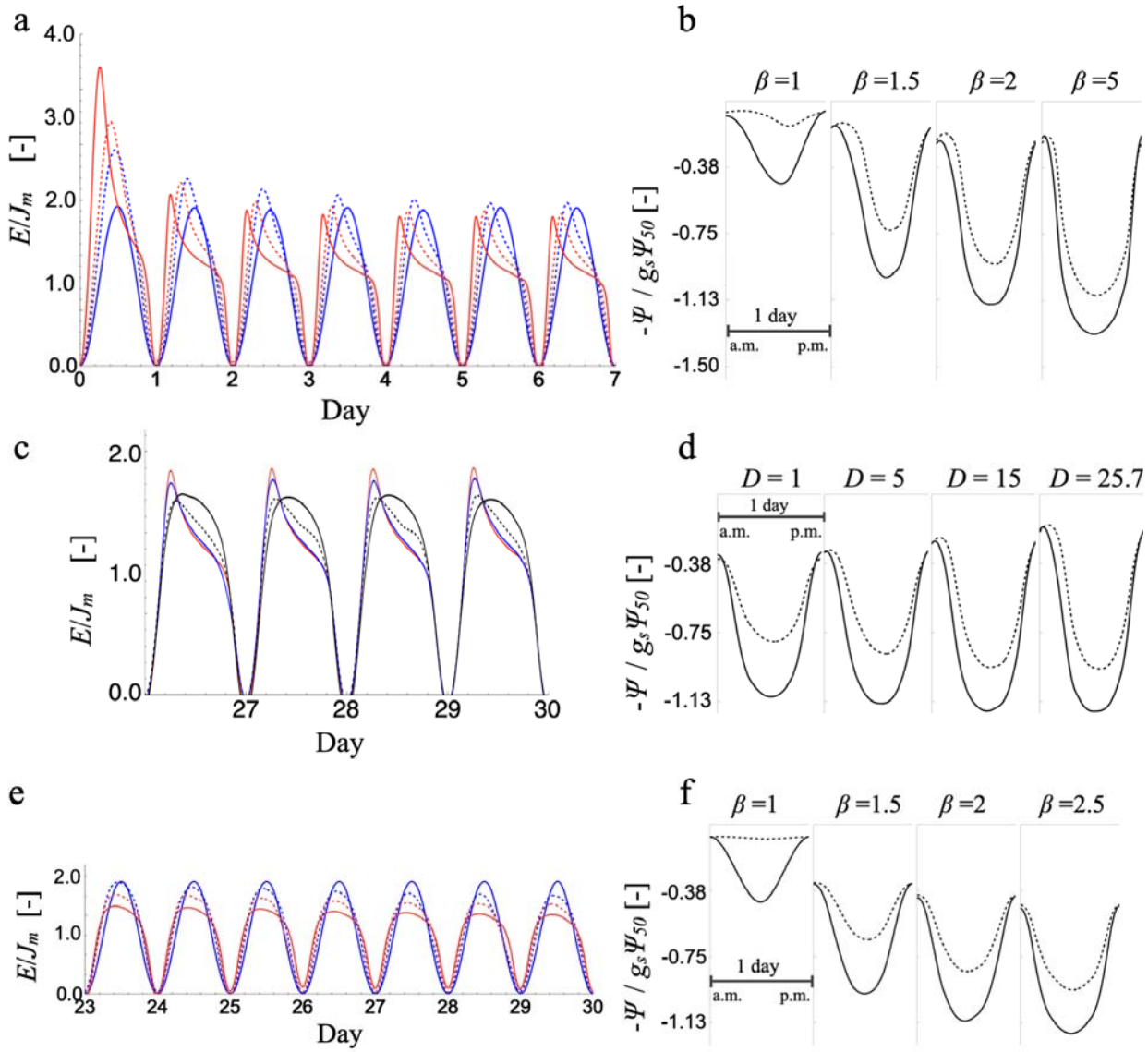

Figure **5.** Emergence of feedforward control of transpiration E and isohydry in the soil-plant system. E (a,c,e) is normalized to the flux recharging the soil domain J_m, and water potential (b,d,f) is normalized to the value at 50% stomatal closure. **a** A parametric sweep across β equal to 1 (blue solid), 1.5 (blue dashed), 2 (red dashed) and 5 (red solid) shows the emergence of feedforward control at high D_o=25.7. **b** Diel course of leaf (solid) and root (dashed) water potentials show a transition from anisohydric to isohydric for the same simulations as in **a** as the drying root surface forces stomata to shut. **c** Decay of feedforward control at β=2.5 as D_o falls from 25.7 (red) to 15 (blue), 5 (black dashed) and 1 (black solid). **d** Diel course of leaf (solid) and root (dashed) water potentials for the simulations in **c** showing no change in the pattern of midday leaf water potentials but greater relaxation at pre-dawn as D_o falls. **e** Parametric sweep across β levels 1 (blue solid), 1.5 (blue dashed), 2 (red dashed) and 2.5 (red solid) showing that at D_o=1 peak broadening replaces the emergence of feedforward control due as β increases. **f** The emergence of isohydry at D_o=1 follows the same pattern as at D_o=25.7.

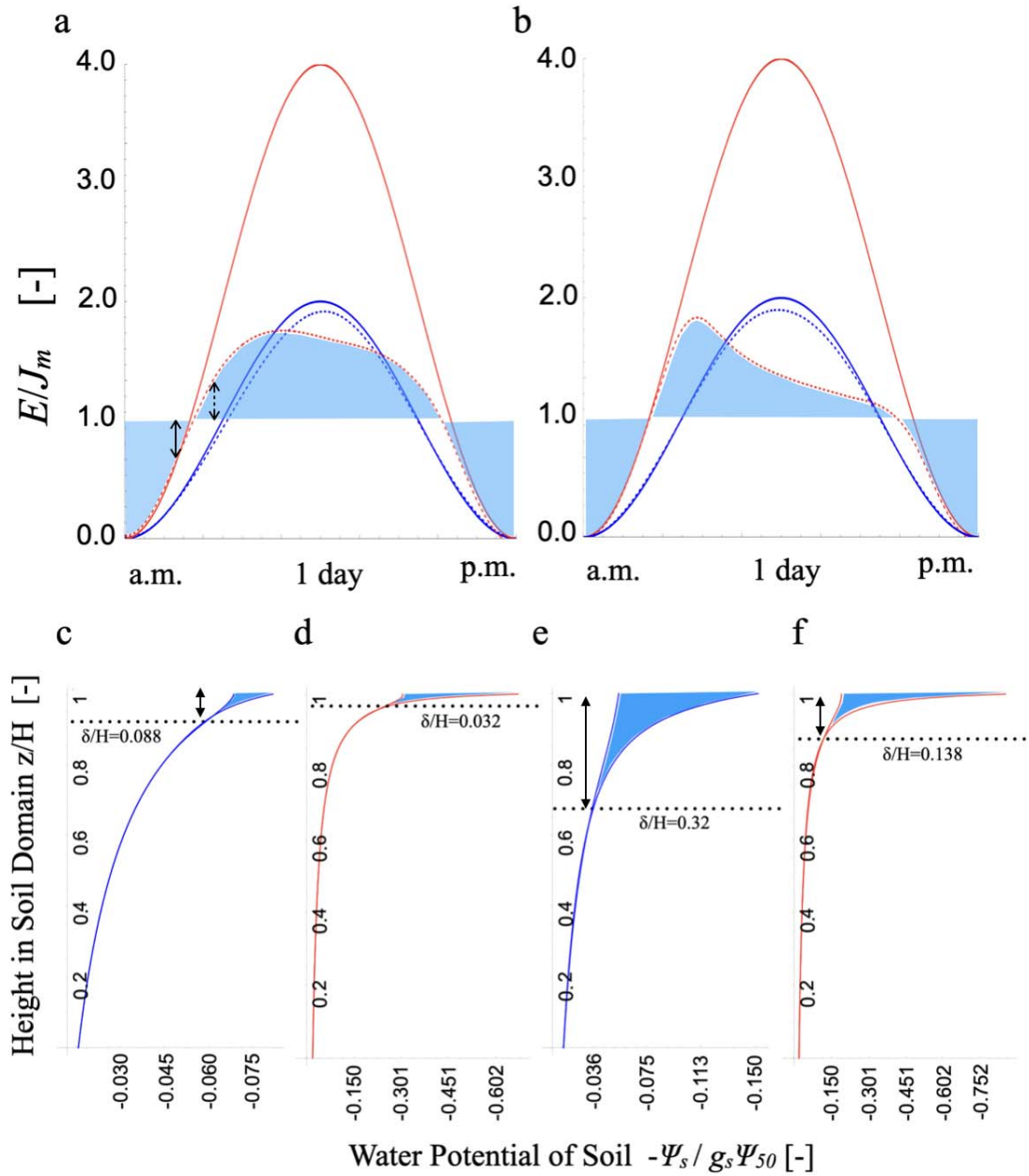

Figure **6**. Diel course of potential transpiration (solid) and actual transpiration E (dashed) normalized to the inward soil recharge flux J_m at β=1 (blue) and β =2 (red) and D_o =1 (**a**) and 25.7 (**b**); light blue shading indicates periods of net recharge (below E= J_m) and discharge (above E= J_m) with respect to the β=2 case, with the heights proportional to the magnitude of the recharge/discharge flux at that instant. **c**,**d**,**e**,**f**: Gradients in soil water potential relative to the leaf water potential for 50% stomatal closure at the daily min and max of E; the light blue region shows the location and potential range for transient release of water (note the difference in potential scales), relative to the damping depth δ, or how deep into the soil domain diel variations are expected to reach. Panels **c,d** correspond to **a,** and **e,f** to **b.** Note that position in the soil domain z and damping depth δ are expressed relative to the domain size H.

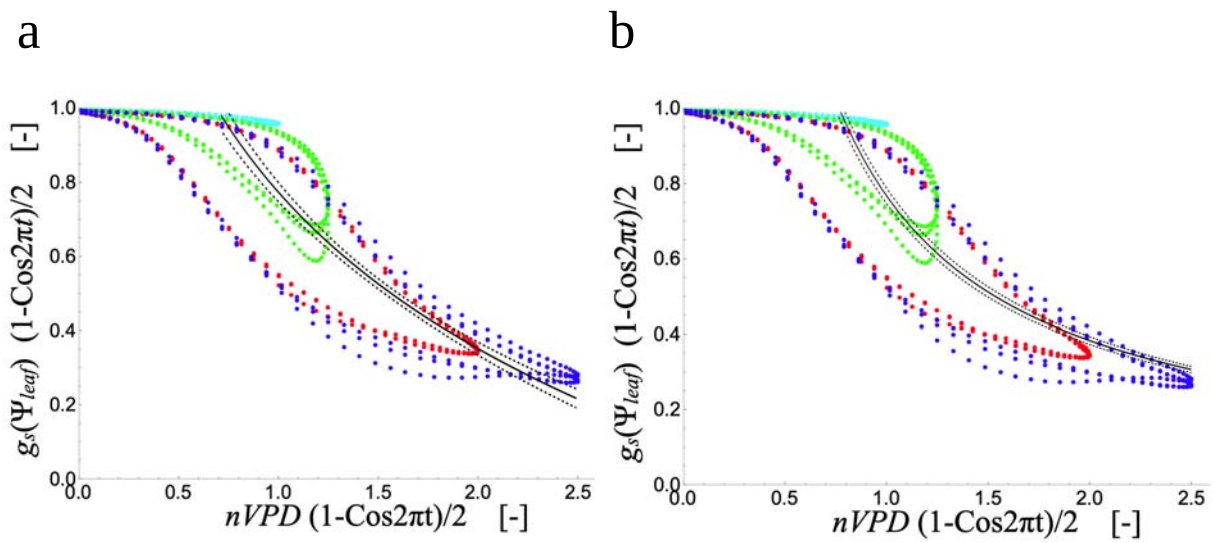

Figure **7**. Fits of simulated diurnal values (hysteretic loops) of stomatal conductance for two contrasting models of stomatal sensitivity to *VPD.* Data are for all four modeled *nVPD* levels (cyan 1, green 1.25, red 2, blue 2.5); black solid lines show the fit and dashed lines the 99% CI. **a** Log-based model: $g_s = g_{s,ref}$ (1- m ln[$nVPD$]), $g_{s,ref}$ =0.78, m = 0.79, adjR^2 = 0.96. **b** Mass-balance based model: $g_s = g_{s,ref} / nVPD$, $g_{s,ref}$ =0.78, adjR^2 = 0.96.

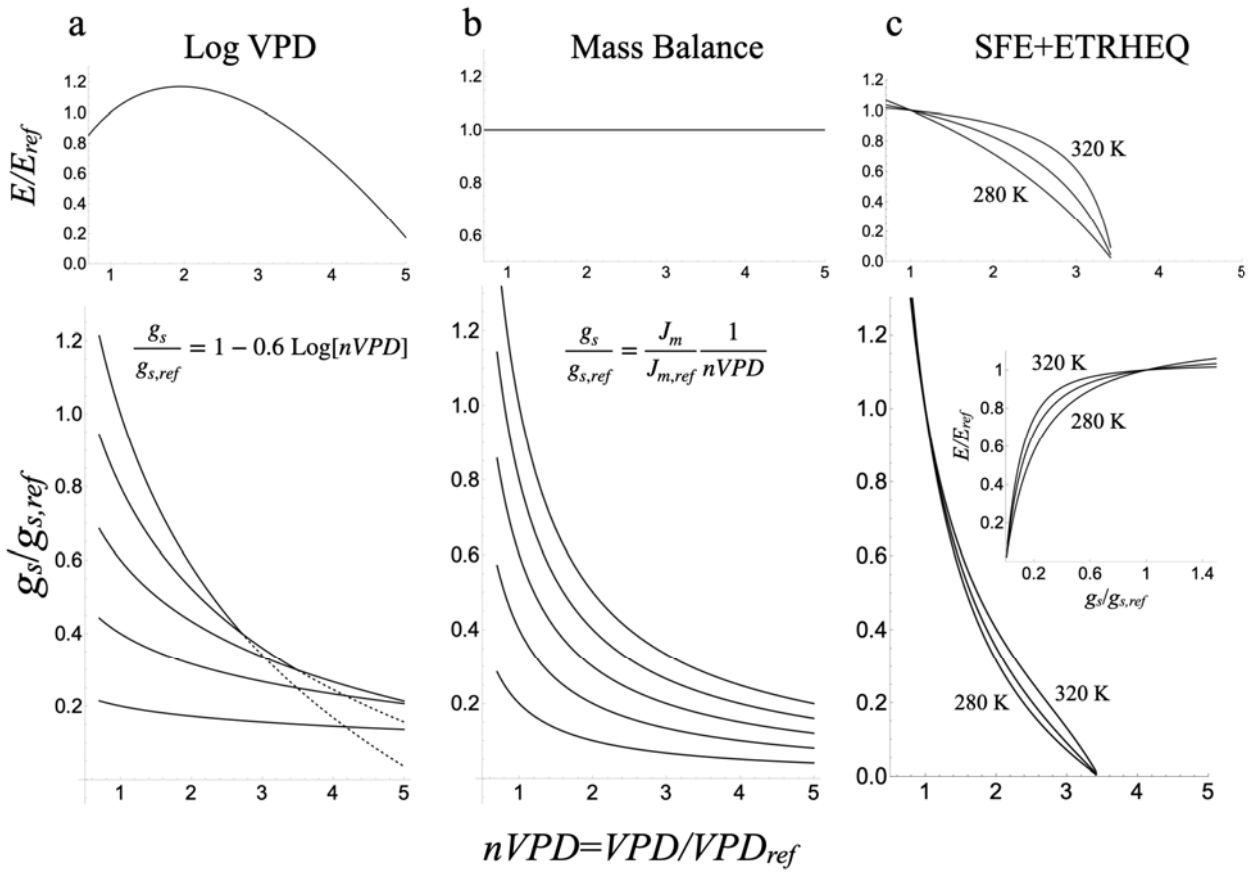

Figure **8**. A comparison of the normalized conductance extinction curves ($g_s/g_{s,ref}$) and transpiration responses (E/E_{ref}) for three simplified models of stomatal responses to soil drying and atmospheric aridity, with 1 kPa as the reference state for *nVPD*. **a** Based on the behavior of the dry sites in figure 2 of Novick *et al.* (2016), as the soil dries in the model $g_s/g_{s,ref} = a$ (1- m ln[*nVPD*]) the intercept a falls from 1 at *nVPD* =1 to 0.2 while the slope m falls from 0.6 to 0.2. Note that the curves representing *nVPD* responses at higher soil moisture are predicted to cross (at the transition from solid to dashed) the curves for lower soil moisture. **b** For the mass balance model $g_s/g_{s,ref} = (J_m/J_{m,ref})$ (1 / *nVPD*), $J_m/J_{m,ref}$ falls from 1 to 0.2 to simulate a falling maximum flux as the soil dries. **c** Under the condition of Surface Flux Equilibrium (SFE), the atmospheric boundary layer approaches a constant RH (and potential *nVPD*) at all heights; responses are shown for air temperatures at two meters above the canopy of 280, 300 and 320 K.

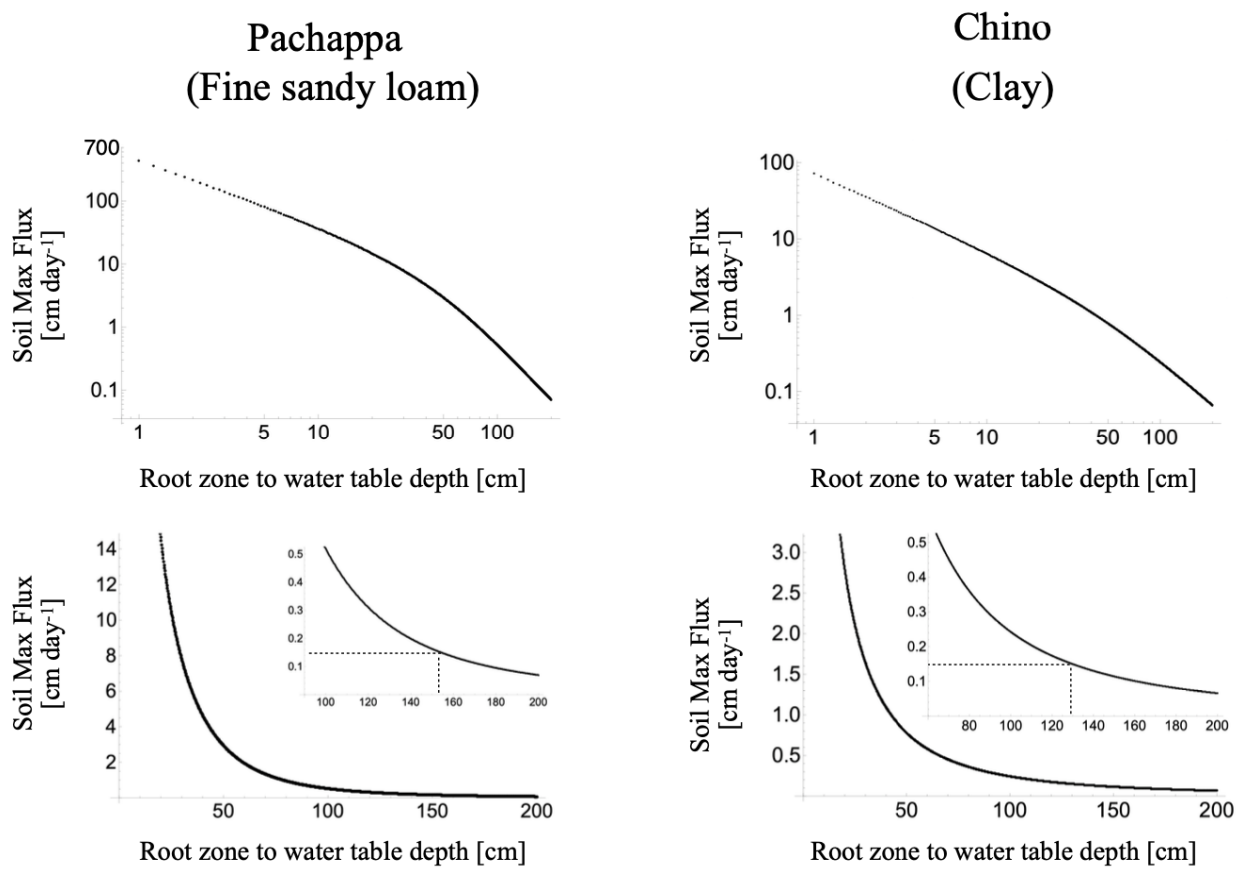

Figure **S1**. Maximum fluxes [cm day^{-1}] for two soils parameterized by Jury *et al.* (1991). Although the saturated conductivities of the two soils differs six-fold, from 2 cm day^{-1} for the clay soil to 12 cm day^{-1} for the more porous fine sandy loam, the maximum soil fluxes converge over longer distances from water table to rooting zone. The flux chosen to match the daily totals for transpiration in the experiment of Drake *et al.* (2018) of 0.15 cm day^{-1} occurs over 130 cm for the clay, and 19% farther (over 155 cm) for the fine sandy loam (inset graphs with dotted lines).

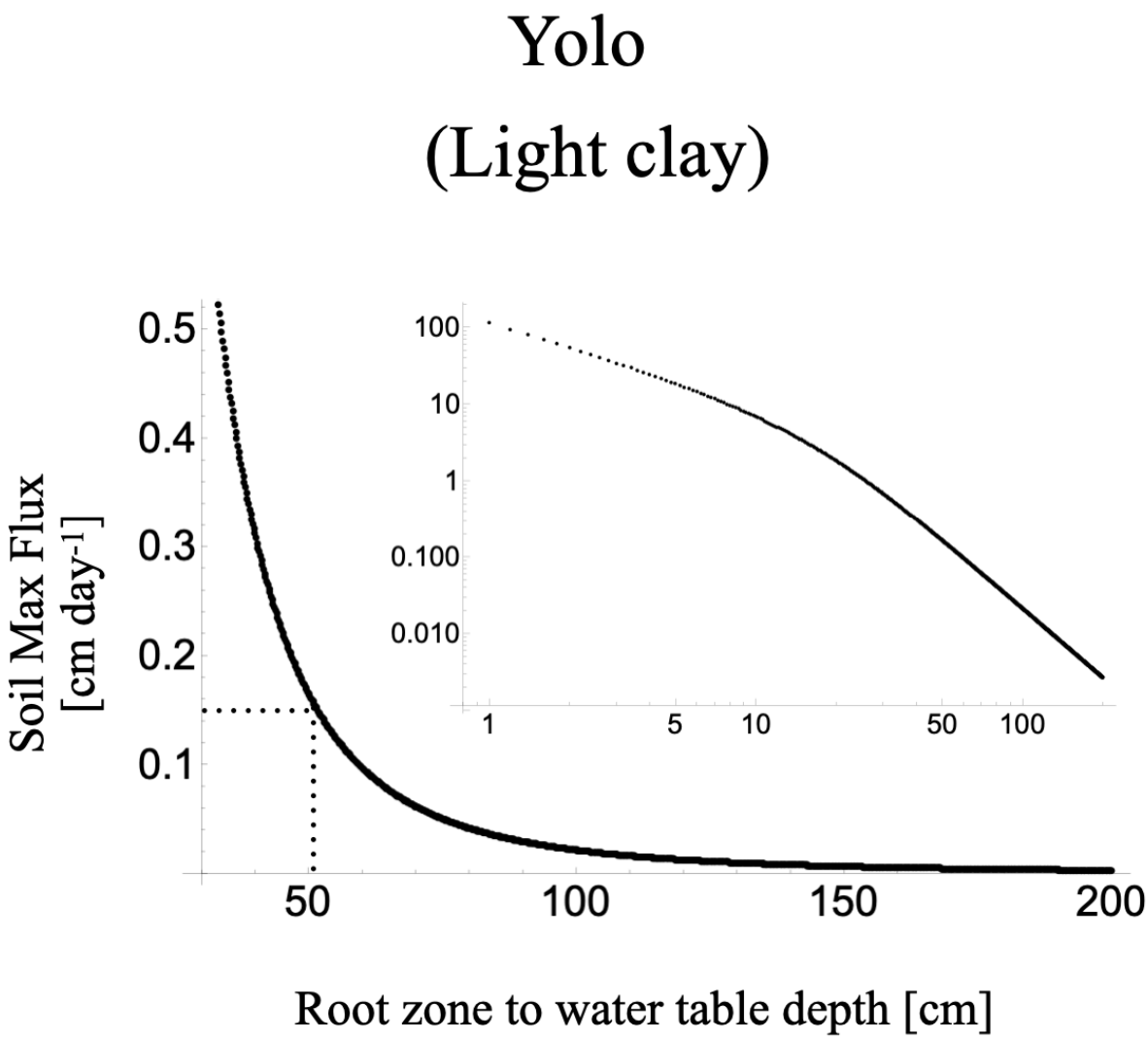

Figure **S2**. Maximum soil flux in the limit of an infinite driving force as a function of the distance from the water table to an uptake surface (i.e., surface evaporation, rooting plane). Data were generated by *eq*. (5) for the case the exponent n = 3, with a = -11 cm and K_s = 9 cm day^{-1}, based on a fit over a range of soil moisture θ from 0.1 to 0.25 by Cowan (1965) to data in Philip (1957) for a Yolo light clay soil reaching field capacity at θ = 0.5.

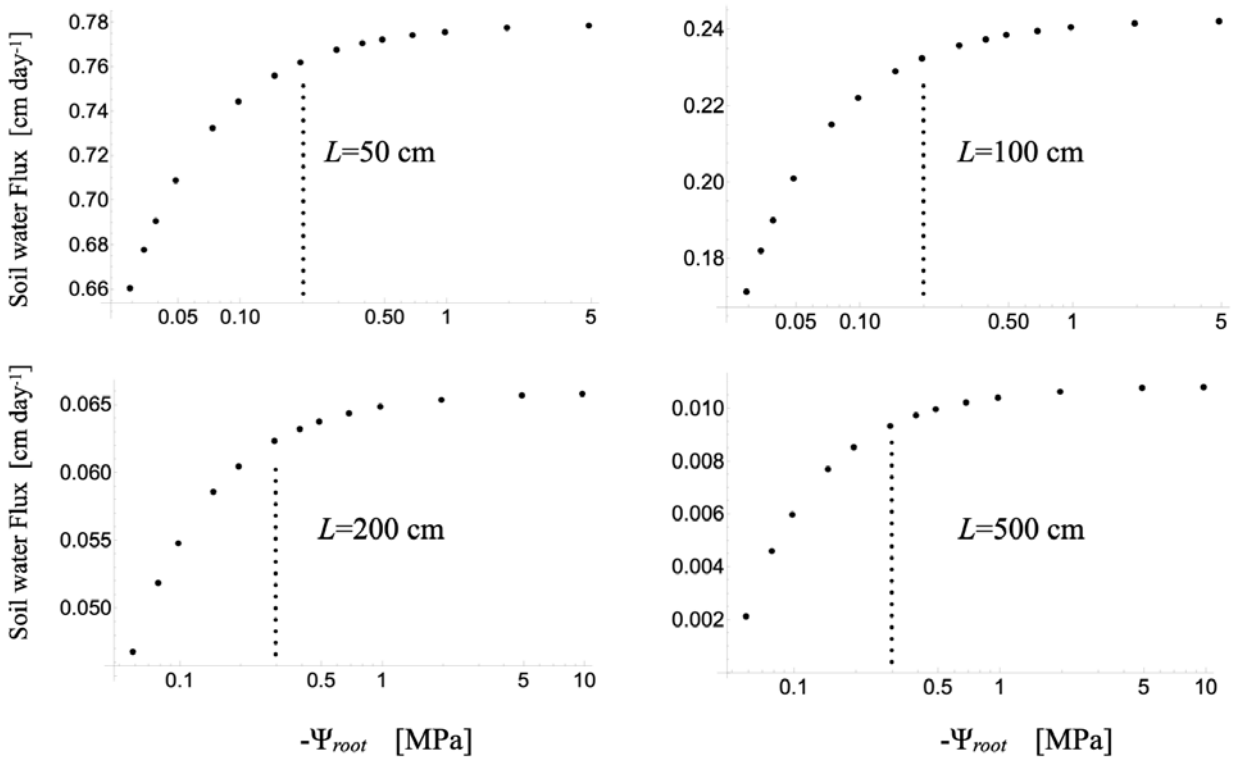

Figure **S3**. Supply curves for the water flux in a Chino clay soil from a water table to an uptake surface (i.e., rooting plane) located a distance *L* above, as a function of the water potential of that surface (Ψ_{root}). As the root pulls with only 0.2 MPa of tension over moderate distances (50 and 100 cm), the flux approaches 95% (dotted vertical lines) of the asymptotic maximum fluxes (Fig. 2) for an infinite driving force. Over longer distances for *L* of 200 to 500 cm, the tension required to reach 95% of the maximum flux increases to a still moderate 0.3 MPa.

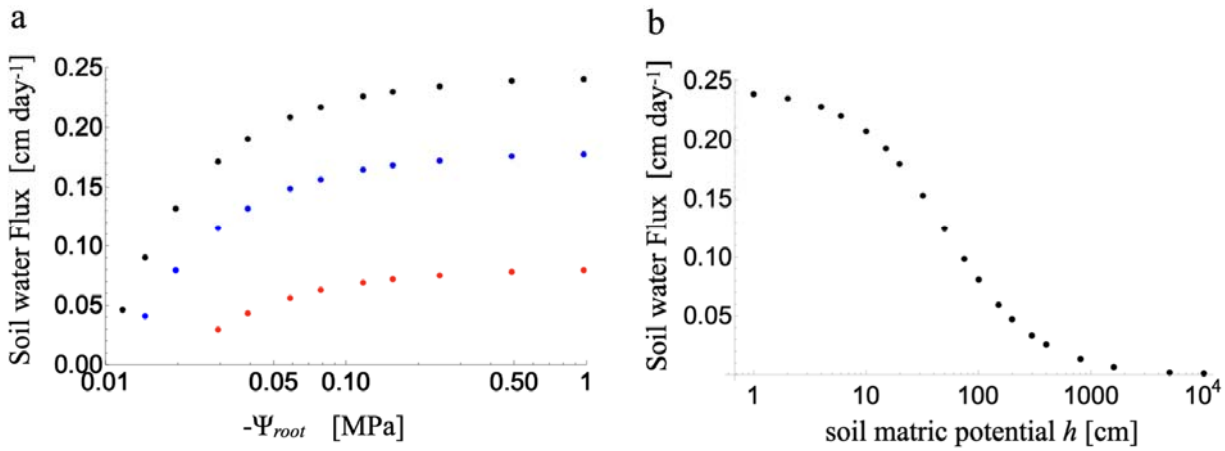

Figure **S4**. Effects of an unsaturated source of deep soil moisture on asymptotic soil water fluxes. **a** Supply curves in a Chino clay soil for a root located *L*=1 meter above a source with a saturated fixed matric potential of 0 (black), versus an unsaturated source held at -20 cm (blue) or -100 cm (Red), as a function of finite root water potentials. All three soil water fluxes reach an asymptotic maximum flux as root water potentials become more negative than approximately -0.2 MPa. **b** Decay of the maximum soil water flux to an infinitely dry sink *L*=1 meter away as a function of the source soil matric potential for a Chino clay soil.

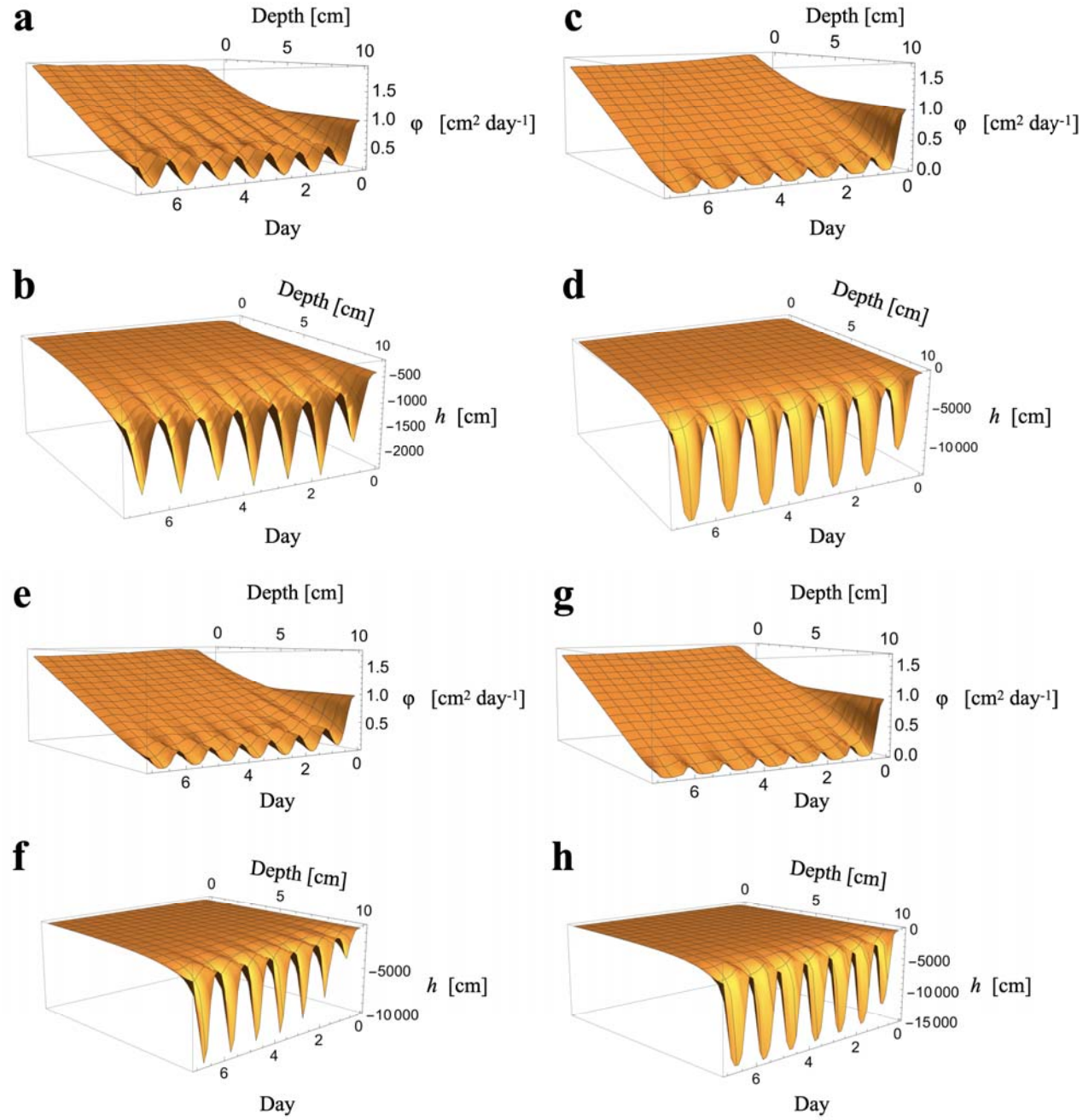

Figure **S5**. Evolution of the potential flux φ for all levels of *nVPD* (**a**,**b** 1; **c**,**d** 2; **e**,**f** 1.25; **g**,**h** 2.5) over the course of the seven-day simulation. Transformation of the results for the potential flux in **a** and **c** into hydraulic head *h* are shown in **b** and **d** respectively. Note that the relationship between water potential and head is approximately 10,000 cm ~ 1 MPa. Note that while the gradients in potential flux evolve to nearly linear with only small diurnal fluctuations at the rooting plane, in the physical matric potential domain all of the large and diurnally varying declines occur in the last centimeter before root absorption.

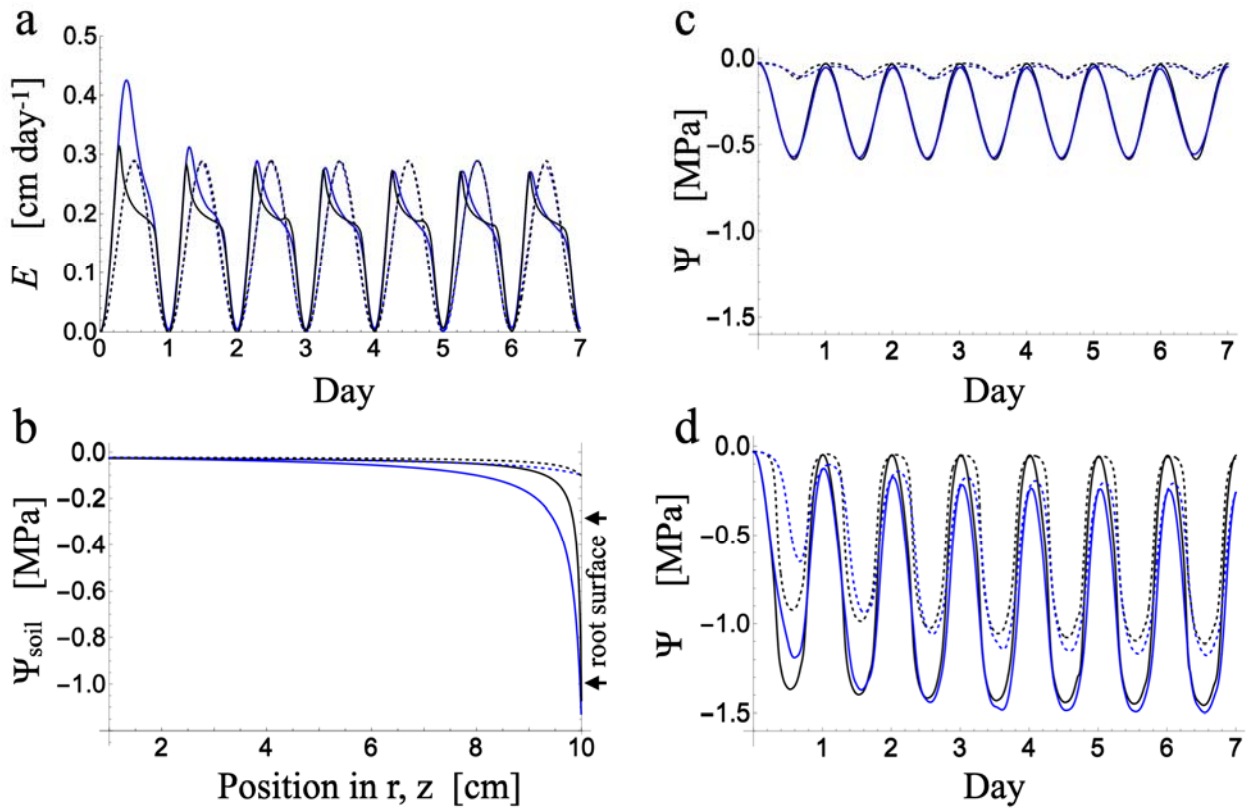

Figure **S6**. Comparison of a cylindrical soil + root domain (black) and the planar geometry adopted in this study (blue) at an *nVPD* of 1 (dashed in **a**,**b** all data in **c**) and 2 (solid in **a**,**b** all data in **d**). **a** In the cylindrical geometry feedforward reductions in *E* are slightly steeper in the a.m. but recover to slightly higher levels in the p.m., but stomata in both geometries respond similarly to the increase in evaporative demand at *nVPD* 2. **b** In the cylindrical domain the gradients start out shallower than in the planar geometry, but become steeper as the flux concentrates in the approach to the root surface, an effect more easily seen at *nVPD* 2 (solid) than 1 (dashed). Despite the difference in the steepness of the gradients, the daily minima of leaf (solid) and root (dashed) water potentials are broadly similar between geometries at both an *nVPD* of 1 (**c**) and 2 (**d**), although under higher diurnal demand overnight recovery is greater in the cylindrical case (**d)**.